A Shared Neural Substrate for Diverse General Anesthetics and Sleep

by

Li-Feng Jiang-Xie

Department of Neurobiology
Duke University

Date:_____

Approved:

_____
Fan Wang, Supervisor

_____
Stephen Lisberger, Chair

_____
Ru-rong Ji

_____
Rebecca Yang

Dissertation submitted in partial fulfillment of
the requirements for the degree of Doctor
of Philosophy in the Department of
Neurobiology in the Graduate School
of Duke University

2019

ABSTRACT

A Shared Neural Substrate for Diverse General Anesthetics and Sleep

by

Li-Feng Jiang-Xie

Department of Neurobiology
Duke University

Date:_____

Approved:

_____
Fan Wang, Supervisor

_____
Stephen Lisberger, Chair

_____
Ru-rong Ji

_____
Rebecca Yang

An abstract of a dissertation submitted in partial fulfillment of the requirements for the degree of Doctor of Philosophy in the Department of Neurobiology in the Graduate School of Duke University

2019

Abstract

Ever since the initial discovery of general anesthetics almost 170 years ago, how general anesthesia (GA) induces loss of consciousness remains a century-long mystery. In addition, whether diverse anesthetic drugs and sleep share a common neural pathway is hotly debated and largely unknown. Previous studies have established that many GA drugs inhibit neural activity through targeting GABA receptors. Here, by using Fos staining, ex vivo brain slice recording, and eventually in vivo multichannel extracellular electrophysiology, we discovered a core ensemble of hypothalamic neurons in and near the supraoptic nucleus, consisting primarily of peptidergic neuroendocrine cells, which are surprisingly and persistently activated by multiple classes of GA drugs. Strikingly, chemogenetic or optogenetic stimulation of these anesthesia-activated neurons (AANs) strongly potentiated slow-wave sleep and prolonged GA, whereas conditional ablation through diphtheria toxin receptor strategy or inhibition of AANs with optogenetics led to reduced slow-wave oscillation in the brain, significant loss of slow-wave and rapid-eye movement sleep, and shortened durations under GA. Together, these findings identify a previously unknown common neural substrate underlying diverse GA drugs and natural sleep, and further illustrate a crucial role of the neuroendocrine system in regulating global brain states.

Contents

List of Tables

List of Figures

Acknowledgements

Thanks first and foremost to my advisor Fan Wang for her generous supports in this project, including acquiring funding, devoting resources, and providing guidance during my graduate studies. I want to express my deepest thanks to my collaborator, Luping Ying, for her generous help on the in vitro brain slice recording, in situ hybridization, immunohistochemistry, and EEG/EMG recording. Without her efforts, it will take much longer for our paper to be published in **Neuron**. I want to thank our Senior Scientist Shengli Zhao for generating CANE viruses and help me got the preliminary data in this study, and also thanks to Bao-Xia Han for genotyping and breeding mice. Thanks to Kafui Dzirasa for providing the training and advices on extracellular recording, and Vincent Provesto for discussion on data analysis. Thanks to Stephen Mague for the training of animal surgery and electrode construction and Gary Lehew for providing the circuit board design in electrophysiology recording. I thank Zhigang He and Chen Wang for providing AAV-DIO-DTR and Dr. Max Kelz for guidance of recording isoflurane responsiveness in brain slices. Also, thanks Satya Achanta for help with some experiments using Propofol. Finally, thanks to the funding agencies, NIH, Keck Foundation, and Brain Research Foundation.

1. Introduction

1.1 Overview

In 1846, more than 170-year ago, William T.G. Morton (1819 –1868) performed the first successfully modern general anesthesia (GA) in Massachusetts General Hospital (Robinson and Toledo, 2012). Ever since then, the procedure of GA has revolutionized surgical procedures in medicine over the past centuries (Franks, 2008; Robinson and Toledo, 2012). Each year, millions of patients worldwide undergo GA for medical treatments. Without it, even a minor surgery would be intolerable for human patients. GA is actually a global brain and body state characterized by (1) unconsciousness, (2) analgesia, (3) amnesia, and (4) immobility while maintaining several vital physiological functions, including cardiovascular, pulmonary, and respiratory systems (Brown et al., 2010; Franks, 2008). However, despite decades of scientific and clinical efforts, the cellular targets and neural circuit mechanisms by which extremely diverse groups of GA drugs all can produce sedation and eventually loss of consciousness (LOC) remain poorly understood (Alkire et al., 2008; Brown et al., 2010; Franks, 2008; Koch et al., 2016; Rudolph and Antkowiak, 2004). Due to this ignorance, patients in the clinics might suffer from intraoperative awareness, brain damage, and even death (Li et al., 2009). As a result, delineating the identities of neuronal targets and the precise neural circuitry that enable GA drugs to induce the unconscious brain state will surly advance our basic

understandings and clinical applications of GA. My dissertation aims to investigate this grand mystery and benefit numerous patients in the hospitals worldwide.

1.2 Molecular targets of general anesthetics

Due to the huge advance of molecular biology in the past century, life scientists realized that identification of molecular or cellular targets of anesthetics might provide crucial cues to this riddle. Within the past several decades, GABA (g-aminobutyric acid) type A ($GABA_A$) receptor has emerged as a principal target for the majority of anesthetics (Franks, 2008). $GABA_A$ receptor is the major contributor of neuronal inhibition and widely expressed throughout the central nervous system. Many drugs have been shown to potentiate GABA induced Cl^- current; in higher doses, they can directly activate $GABA_A$ receptors without anesthetics (Franks, 2008). Furthermore, specific genetic mutations in the receptors would largely reduce the potency of anesthetics (Belelli et al., 1997; Mihic et al., 1997). On the other hand, there are also non-GABAergic anesthetics, such as ketamine, which targets the NMDA receptor to reduce the excitatory action of glutamate, and dexmedetomidine, which binds to alpha-2 (a2) adrenergic receptors and inhibits the norepinephrine release from locus coeruleus (Franks, 2008). Furthermore, numerous volatile anesthetics are shown to facilitate the opening of two-pore-domain background potassium channels and hyperpolarize the neurons (Franks, 2008; Franks and Lieb, 1988). Together, these results lead to the idea that different GA drugs work by exerting differentiated inhibitory impacts on the

nervous system, although the particular loci (if present) that anesthetics target to induce unconsciousness is still elusive.

In recent years, a few studies have suggested the existence of anesthetic-activated cells in several brain regions, including hypothalamus, lateral habenula, and brainstem using either immediate early gene markers c-fos, or ex vivo brain slice recording (Gelegen et al., 2018; Lu et al., 2008; Moore et al., 2012; Zhang et al., 2015b). However, no study so far has provided conclusive evidence of anesthetic-activated neurons with in vivo electrophysiology, and whether there is a common neural substrate activated by different classes of GA drugs is unknown.

1.3 The relationship between general anesthesia and sleep

The overlap between GA and endogenous sleep-wake circuitry is also actively debated. Examination of brain oscillations revealed that, although different anesthetics produce distinct patterns of electroencephalography (EEG) that may not be observed in natural sleep, one of the shared features between deep sleep and GA is the enhancement of slow-delta (0.5–4 Hz) oscillations (Akeju and Brown, 2017; Franks, 2008; Rudolph and Antkowiak, 2004). In addition, body temperature and breathing rate both decrease in GA and deep (slow-wave) sleep, while the sensory thresholds increase in these two states (Franks, 2008). Notably, sleep deprivation results in increased homeostatic pressure to sleep and enhances the potency of GA (Tung et al., 2002). The recovery process from sleep deprivation can also take place during GA (Tung et al., 2004).

Interestingly, it has been shown that the sensitivity to volatile anesthetic Isoflurane is strongly correlated with the propensity to sleep even in fruit fly Drosophila (Kottler et al., 2013). On the other hands, numerous types of wake-promoting cells in the brain are required for emergence from GA, including dopaminergic neurons in the ventral tegmental area (Taylor et al., 2016), orexin neurons in lateral hypothalamus (Kelz et al., 2008), noradrenergic cells in locus coeruleus (Vazey and Aston-Jones, 2014), and cholinergic neurons in basal forebrain (Pal et al., 2018). However, the exact biological substrate promoting both GA and sleep remains to be identified.

In the past two decades, there are substantial progresses in the field of sleep research (Kilduff and Dan, 2017). One of the most striking discoveries is that multiple types of peptidergic neurons, which usually co-release peptides and small molecule transmitters (glutamate or GABA), participate in regulating sleep across different species, including fly (Toda et al., 2019), fish (Lee et al., 2017), and rodents (Chung et al., 2017; Jego et al., 2013). Compared to fast transmitters, neuropeptides exert wider spreading and longer-lasting effects, which are ideally suited to regulate global brain state. However, the potential roles of neuropeptides in GA are largely an uncharted territory, and whether there are common neuropeptides engaged in both sleep and GA is unexplored.

1.4 Contribution to the fields of GA and sleep

Here, I reasoned that neurons activated by multiple different GA drugs may represent a shared substrate between GA and sleep. Using a combination of immediate early gene c-fos expression, ex vivo brain slice, and in vivo extracellular recordings, we uncovered a hypothalamic neuronal population, which unexpectedly consists primarily of neuroendocrine cells, that are surprisingly and persistently activated by multiple distinct GA drugs. With our recently developed capturing activated neuronal ensembles (CANE) technology (Sakurai et al., 2016), we were able to precisely label, characterize and manipulate these anesthesia-activated neurons (AAN). In freely behaving mice, optogenetic (Boyden et al., 2005) and chemogenetic (Roth, 2016) activation of AAN were sufficient to strongly potentiate slow-wave sleep (SWS) and GA. Importantly, conditional ablation of AAN resulted in significant decline of slow-wave power and loss of both SWS and REM (rapid eye movement) sleep, while acute inhibition of AAN shortened the duration of GA. Together, our results revealed a previously unrecognized function of neuroendocrine cells, which are known for their role of releasing hormones, in regulating both GA and natural sleep.

2. Discovery of anesthesia-activated neurons (AANs)

2.1 Whole-brain Fos immunohistochemistry

Fos in an immediate early gene that is generally used as an indicator for neuronal activation. When the neuron fires action potentials, a huge calcium influx will trigger numerous intracellular signaling cascades that eventually turn on Fos expression. (Morgan and Curran, 1989). Fos has been successfully applied as a reliable neuronal activity marker in the context of different behavior assays, including learning, memory (Liu et al., 2012), emotion (Kung et al., 2010), pain (Harris, 1998), and sleep (Chung et al., 2017). We decided to utilize Fos expression as a tool as to search for anesthesia-activated neurons (AANs) in the brain. Initially, mice were subjected to either isoflurane-oxygen anesthesia or to oxygen exposure alone (control) for two hours, followed by examining the brain with Fos immunohistochemistry. The two-hour time window is chosen based on the temporal dynamics of the Fos protein, which typically reaches the highest expression level around 1.5~2.5 hour after initial neuronal activation (Lin et al., 2008).

As compared to control condition, Fos expression throughout the brain was dramatically diminished across the neocortex, thalamus, and basal ganglia, and brain stem under isoflurane GA, but I observed there are three distinct clusters of strong Fos^+ neurons, one group located in ventral hypothalamus, other two populations reside in central amygdala (CeA), and bed nucleus of the stria terminalis (BNST). Here, my dissertation primarily focuses on the cluster of Fos^+ neurons in ventral hypothalamus

(Figure 1), a region containing neurons regulating sleep-wake cycles (Scammell et al., 2017; Weber and Dan, 2016). Notably, most of the AANs (more than 80% of Fos^+ cells) surprisingly resided at the upper corner of the optic chiasm, extending through the anterior-to-posterior axis of the ventral edge of the hypothalamus, which is canonically defined as the supraoptic nucleus (SON) (Figure 1), located actually posterior to the ventrolateral preoptic nucleus (VLPO) (Kroeger et al., 2018). There was also a sparse population of AANs scattered from ventral preoptic area (POA) to areas dorsal to posterior SON under isoflurane (Figure 1); we refer to these regions collectively as the paraSON area. These results come as a surprise since previous research suggests there are Fos^+ neurons specifically located in VLPO (Moore et al., 2012) under GA, our data suggested the majority of AANs actually resided in SON.

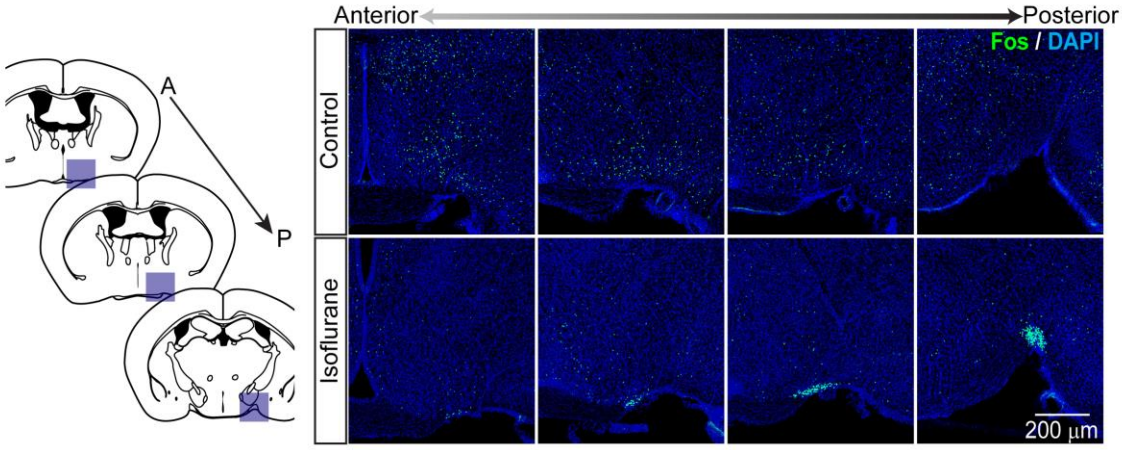

Figure 1. Discovery of general-anesthesia-activated neurons (AAN) in hypothalamus with Fos staining.

Left, schematics of interested regions on the brain atlas. A, anterior; P, posterior. Right, representative patterns of Fos^+ neurons (approximately 0 mm to -1.2 mm from bregma) after 2-hour control (oxygen) versus isoflurane exposure (1~1.2% Isoflurane mixed with oxygen) from n = 4 pairs of mice.

2.2 In vivo multi-channel extracellular recording with simultaneously brain state monitoring

Although Fos is considered as a reliable marker for neuronal activity, other cellular events (such as signaling of neurotrophic factors, or activation of protein kinase A) might drive Fos expression without eliciting neuronal action potentials (Lin et al., 2008). To gain more direct evidence that AAN indeed increases firing in vivo under GA, we have to record well-isolated single-unit activity in AAN region with simultaneous monitoring of local field potentials (LFP) in frontal cortex (a region crucial for conscious awareness) and electromyography (EMG) in neck muscle (as an indicator of movement) ahead, during, and after GA. To achieve this goal, we construct custom neural probes that could perform single-unit, LFP and EMG recordings across multiple brain regions at the same animal concurrently (Dzirasa et al., 2011).

With these neural probes, I successfully recorded around 90 high-quality single-unit in AAN region (Figures 2-3; n = 89 neurons from 7 mice). The neurons recorded were further classified into three general categories based on their responsiveness toward isoflurane exposure (1~1.2 %, 10 minutes). While the majority of recorded cells were either suppressed (36%), or weakly modulated (53%) by isoflurane infusion, we did discover a minor population of neurons (11%, 10 out of 89) with very low baseline activity were strongly and persistently activated under GA (Figures 3). Interestingly, a significant fraction of these activated cells (60%, 6 of these 10) increased firing rates even before the brain state transitioned from wakefulness to the loss of consciousness state

(LOC) as determined by the enhancement of slow-wave oscillation in frontal cortex LFP and minimal muscle activity in EMG (Figure 3; Figure 4), and the majority of cells (70%, 7 of the 10) reduced firing rate before the animal emerged from GA (Figure 3; Figure 4). These results suggested that GA indeed elicits robust and persistent firing of AAN in vivo. To our knowledge, this is the first in vivo demonstration the existence of anesthesia-activated cells in the freely behaving animals. Instead of non-specifically silencing the neuronal activity across entire central nervous system through targeting $GABA_A$ receptors, our results clearly identify a novel set of neurons that are strongly activated by GA. This discovery suggests a previously unknown mechanism of GA which will open a new gateway for anesthesia research.

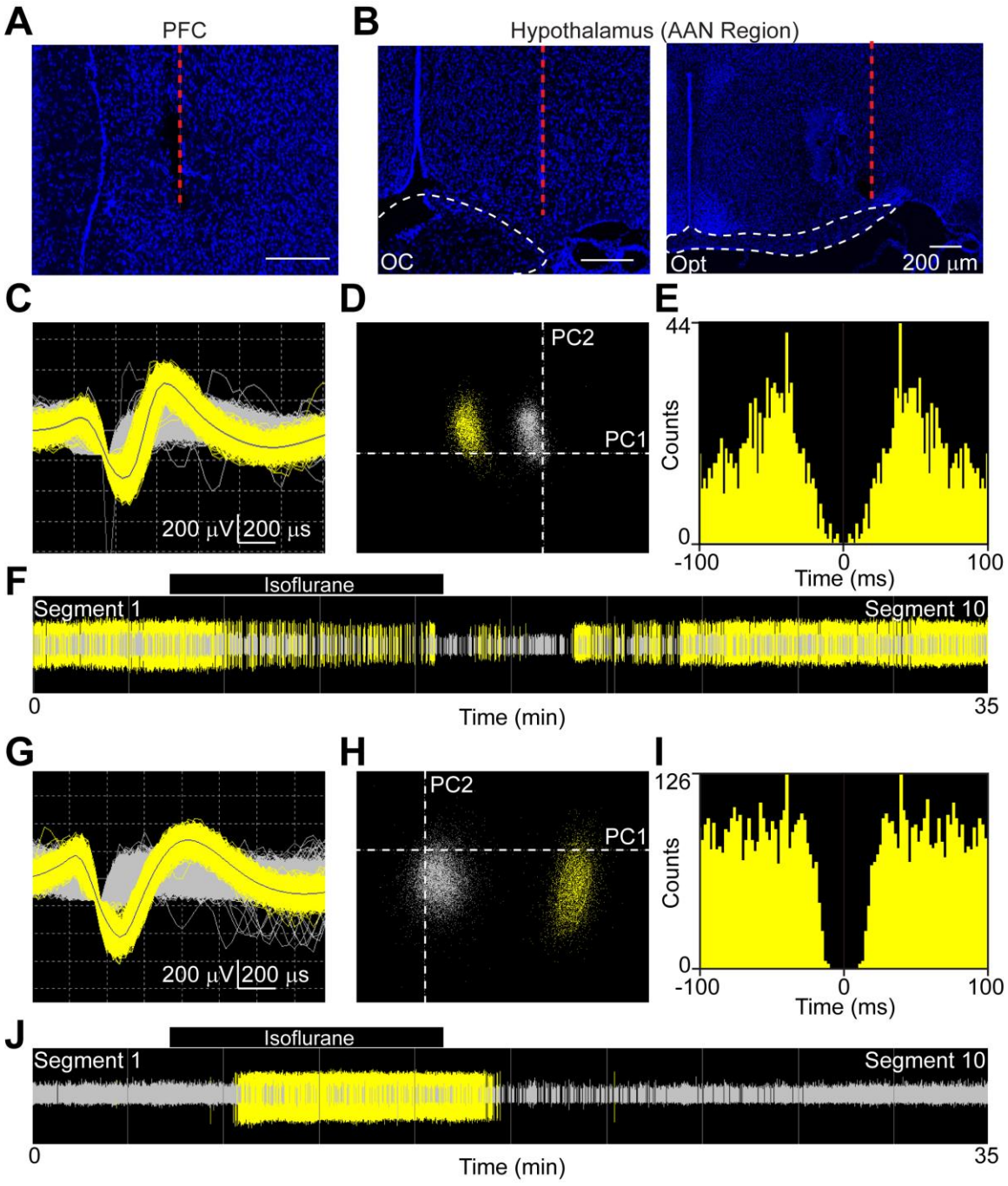
A
PFC
B
Hypothalamus (AAN Region)
OC
Opt
200 µm
C
200 µV
200 µs
D
PC2
PC1
E
44
Counts
0
-100
0
100
Time (ms)
F
Isoflurane
Segment 1
Segment 10
0
Time (min)
35
G
200 µV
200 µs
H
PC2
PC1
I
126
Counts
0
-100
0
100
Time (ms)
J
Isoflurane
Segment 1
Segment 10
0
Time (min)
35

Figure 2. Microwire electrode placement and examples of well-isolated single-unit AAN activity with Plexon Offline Sorter.
(A-B) Example of electrode track (Red dashed line) in frontal cortex and the AAN region.
(C-F) An example of isoflurane-suppressed neuron. (G-J) an example of isoflurane-activated neuron. Yellow, isolated unit; Gray, noise. (C), (G) Waveforms. (D), (H) Cluster view in principle component space. PC1, principle component 1; PC2, principle component 2. (E), (I) Autocorrelogram. (F), (J) Identified spikes across recording session.

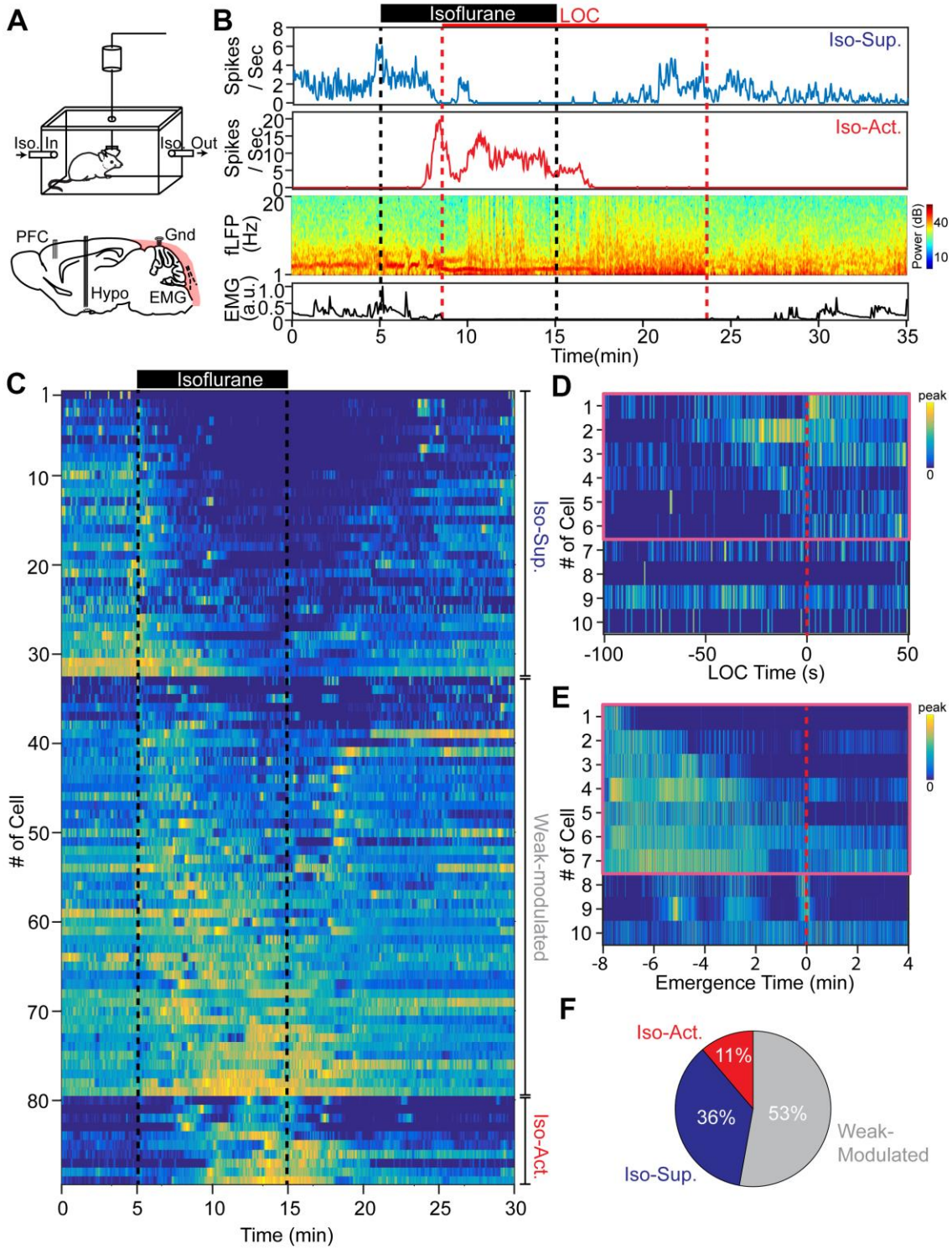
A
Iso. In
Iso. Out
PFC
Gnd
Hypo
EMG
B
Isoflurane
LOC
Iso-Sup.
Iso-Act.
Spikes / Sec
fLFP (Hz)
Power (dB)
EMG (a.u.)
Time(min)
C
Isoflurane
# of Cell
Iso-Sup.
Weak-modulated
Iso-Act.
Time (min)
D
peak
# of Cell
LOC Time (s)
E
peak
# of Cell
Emergence Time (min)
F
Iso-Act.
11%
36%
53%
Weak-Modulated
Iso-Sup.

Figure 3. Simultaneous in vivo extracellular recording of hypothalamic neurons in the AAN region and the brain states before, during, and after GA.
(A) Schematics of recording chamber and electrode placement. Iso, isoflurane; PFC, prefrontal cortex; EMG, electromyography; Gnd, ground. (B) Representative isoflurane-suppressed (Iso-Sup.) and isoflurane-activated (Iso-Act.) neuron. Top two panels, spike-rate of the example neuron; third, frontal cortex LFP (fLFP); bottom, EMG. Black dashed lines mark the duration of isoflurane exposure. Red dashed lines indicate the period of loss-of-consciousness (LOC). (C) Activity profile of all neurons recorded (n = 89). The spike rate of each neuron was normalized by its peak firing rate. (D-E) Activities of isoflurane-activated neurons (raw spike trains convolved with 1-s Gaussian kernel) aligned with the time when mice lose consciousness (D) or emerge from GA (E). Purple square highlights the neurons that increased firing rate before LOC (D), or decreased firing rate ahead of emergence (E). (F) Categorize the neuronal population based on its response toward isoflurane. n = 89 neurons across 14 sessions from 7 mice.

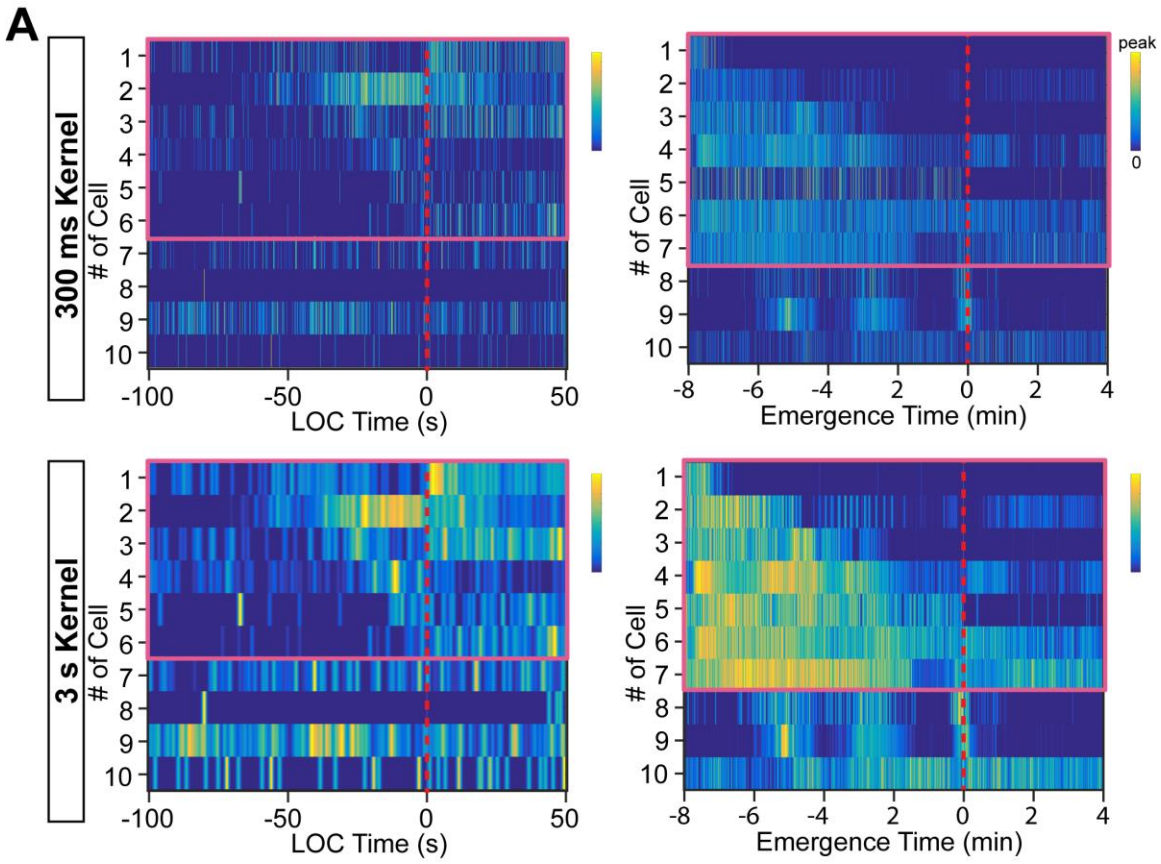

Figure 4. Activities of isoflurane-activated neurons estimated with different size of Gaussian kernels aligned with LOC and Emergence. (A) Top, 300-ms kernel; bottom, 3-s kernel. LOC, loss of consciousness.

2.3 Molecular signatures of AAN

After the initial identification of AAN, we next want to further characterize the underlying neurochemical signatures, which might provide important clues to its biological functions. Based on previous literature, it has been known that volatile anesthetics and natural slow-wave sleep activated hypothalamic GABAergic and/or galaninergic neurons in POA (Moore et al., 2012; Sherin et al., 1998). On the other hand, SON is known to contain peptidergic neuroendocrine cells that mainly produce arginine vasopressin (AVP, also known as antidiuretic hormone, ADH), prodynorphin (Pdyn) or oxytocin (OXT) (Ludwig and Leng, 2006; Mutsuga et al., 2004). Here, using two-color in situ hybridization in which AAN were identified with Fos RNA probe (induced by isoflurane GA), we found that 45.20% scattered AAN in the paraSON region were $vGat^+$, while 44.67% were $vGlut2^+$ (Figure 5, Table 1). Thus, the paraSON AAN contained both inhibitory and excitatory cells. However, AAN located within SON were largely but weakly $vGlut2^+$ (Ponzio et al., 2006) (95.39%). Further investigation revealed around 80% AAN in SON expressed AVP and Pdyn (85.95% for AVP; 81.22% for Pdyn), while 10.87% SON AAN were $Galanin^+$ (Figure 6, Table 1). AAN were largely non-overlapping with the high-level (bright) OXT expressing SON cells. However, under GA, there appeared a population of low (dim) level of oxytocin expression SON cells that was not present in control (un-anesthetized) conditions (Figure 7). Interestingly, 89.26% AAN showed such dim OXT expression (Figure 6). It has been known that SON AVP cells

express very low level of oxytocin in basal condition (Leng, 2018). These results suggest that GA may induce OXT mRNA expression in AAN. Overall, the hypothalamic AAN population is largely composed of peptidergic neurons (which are also weakly vGlut2^{+}) in SON and sparsely distributed GABAergic and glutamatergic cells in paraSON.

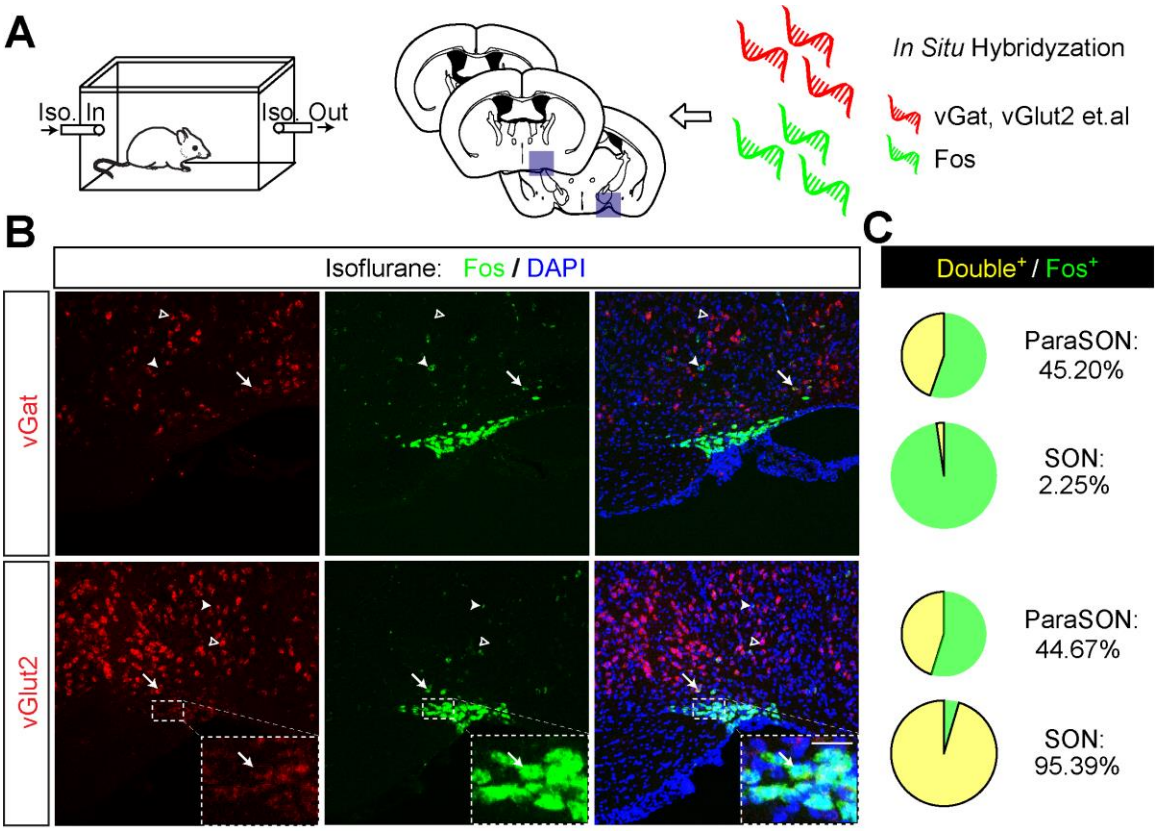

Figure 5. Molecular signatures of AAN (fast transmitters).
(A) Experimental procedure of two-color in situ hybridization on AAN. vGat, vesicular GABA transporter; vGlut2, vesicular glutamate transporter 2. (B) Representative images of two-color in situ hybridization between Fos (green) that marks AAN and following probes (red): vGat, vGlut2. Arrow, open arrowhead and solid arrowhead indicating double$^+$, probe$^+$ only and Fos$^+$ only cells, respectively. (C) Pie chart of percentage of AAN (Fos+) colocalized with each probe in SON and paraSON region. Neurons were from 7-23 sections from 2-3 mice for each pair of condition.

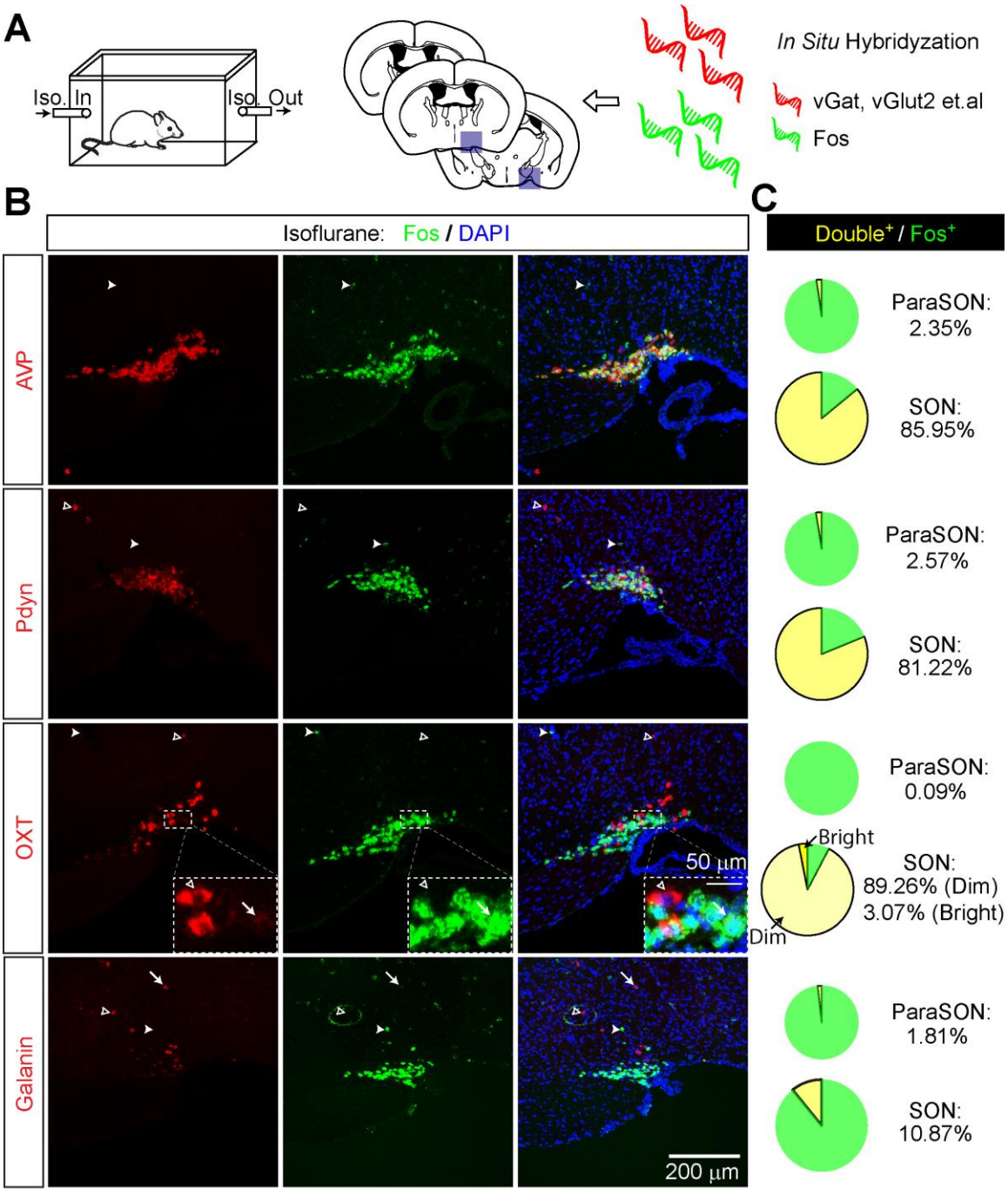
A
Iso. In
Iso. Out
In Situ Hybridyzation
vGat, vGlut2 et.al
Fos
B
Isoflurane: Fos / DAPI
AVP
Pdyn
OXT
Galanin
50 μm
200 μm
C
Double+ / Fos+
ParaSON:
2.35%
SON:
85.95%
ParaSON:
2.57%
SON:
81.22%
ParaSON:
0.09%
Bright
SON:
89.26% (Dim)
3.07% (Bright)
Dim
ParaSON:
1.81%
SON:
10.87%

Figure 6. Molecular signatures of AAN (neuropeptides).
(A) Experimental procedure of two-color in situ hybridization on AAN. AVP, arginine vasopressin; Pdyn, prodynorphin; OXT, oxytocin.
(B) Representative images of two-color in situ hybridization between Fos (green) that marks AAN and following probes (red): AVP, Pdyn, OXT, and Galanin. Arrow, open arrowhead and solid arrowhead indicating double$^+$, probe$^+$ only and Fos$^+$ only cells, respectively. (C) Pie chart of percentage of AAN (Fos$^+$) colocalized with each probe in SON and paraSON region. Neurons were from 7-23 sections from 2-3 mice for each pair of condition.

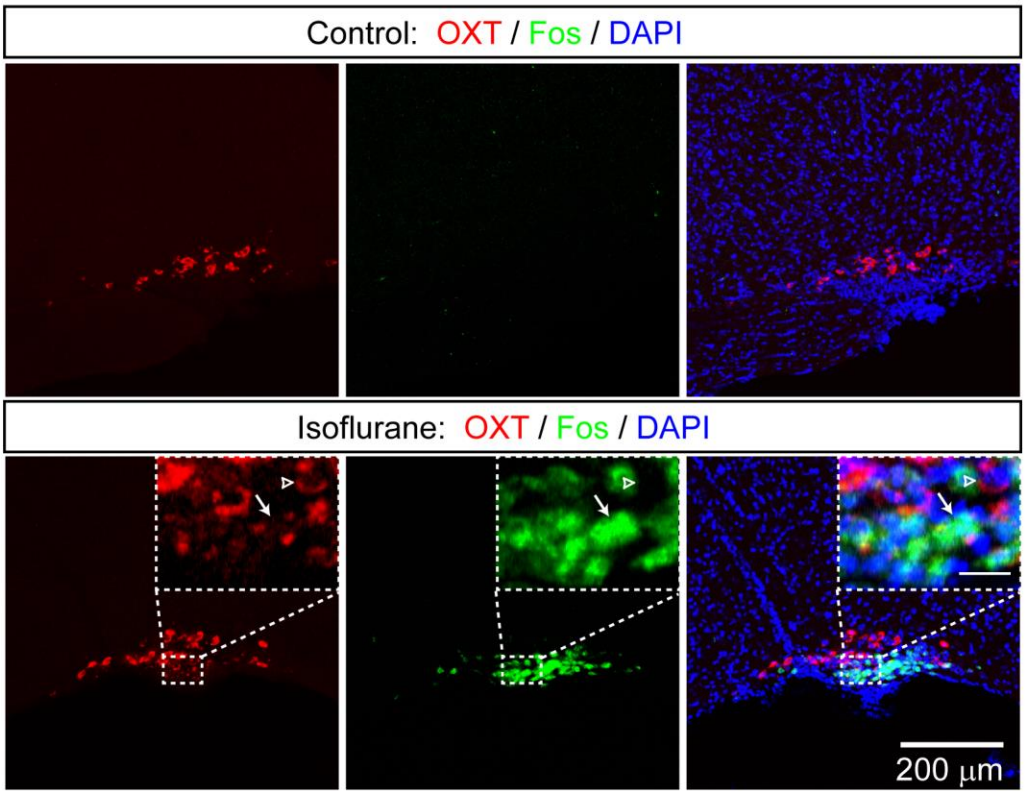

Figure 7. Isoflurane anesthesia induces dim oxytocin mRNA expression in SON.
Top, unanesthetized (home cage) control; bottom, isoflurane anesthesia. Green, Fos; red: OXT, oxytocin; blue, DAPI. Arrow, open arrowhead indicating double+ and OXT+-only cells, respectively.

Table 1. Primers for in situ hybridization.

Primer	Sequence	SOURCE	IDENTIFIER
c-fos	*F*: AGAATCCGAAGGGAACGG	Allan Brain Atlas	Fos-RP_080109_01_B10
	R: GGAGGCCAGATGTGGATG		
vGlut2	*F*: CAAGAAGGTGCGCAAGACGCGTACACC	Bellavance et al., 2017	N/A
	R: TGCCCAAGCATTTCACAAAACACTGC		
vGat	*F*: GGCCACCTCCGTGTCCAACAAGTCC	Bellavance et al., 2017	N/A
	R: GAATTCGCTGGGCTGCTGCATGTTG		
Vasopressin (AVP)	*F*: CCGAGTGCCACGACGGTTT	Allan Brain Atlas	Avp-RP_070129_04_B12
	R: TTCCATGCTGTAGGGGCGAG		
Prodynorphin (Pdyn)	*F*: AGGAAAAGTTCAGGGGTCTCTC	Allan Brain Atlas	Pdyn-RP_050505_04_B03
	R: TCTCACAGTTCCCATGCAATAC		
Oxytocin (OXT)	*F*: CACCTACAGCGGATCTCAGAC	This paper	N/A
	R: AGACACTTGCGCATATCCAGG		
Galanin	*F*: ATCCTGCACTGACCAGCC	Allan Brain Atlas	Gal-RP_050303_02_F03
	R: TTGGCTTGAGGAGTTGGC		

3. AAN represent a common substrate targeted by multiple distinct GA drugs

3.1 Capturing anesthesia-activated neurons with CANE technology

A critical issue needed to address is whether the AAN we discovered here represents a common target for diverse GA drugs, or different anesthetics just recruit distinct neuronal ensembles. To answer this question, we employed a new viral-genetic technology that can specifically and permanently label AAN, Capturing Activated Neuronal Ensemble (CANE) technology (Sakurai et al., 2016). This strategy is ideally suited to express any desired transgene in Fos^{+} neurons (Figure 8A). CANE system has two major components, (1) the generation of Fos^{TVA} knock-in mice, in which the destabilized TVA (dsTVA) receptor is placed under the endogenous control of Fos gene. In addition, the dsTVA receptors only transiently express on the cellular membranes due to its unstable nature, and the time-scale of expression nicely matches the temporal dynamics of Fos protein, (2) the engineering of pseudo-typed lentivirus (CANE-LV) that could selectively and efficiently infect Fos^{+} neurons in the Fos^{TVA} knock-in mice. With CANE technology, we can have a reliable genetic access to AAN. Our first goal is to precisely label AAN with red fluorescent protein, mCherry.

We subjected Fos^{TVA} mice to two hours isoflurane (1~1.2%) GA, followed by co-injection of CANE-LV-Cre with Cre-dependent AAV-DIO-mCherry into AAN region (Figure 8B). One month later after the fluorescent marker fully expressed, the mice were

re-exposed to two-hour of isoflurane GA again, and the activated neurons were visualized with Fos staining with green color. We found that 92.72% of CANE-mCherry labeled neurons in SON and 73.87% in paraSON re-expressed Fos^+ after second isoflurane GA, suggesting that the same ensemble of AAN was re-activated by the repeated GA (Figure 9). As a proof of principle, our data indicated that we could reliable label the AAN with CANE technology.

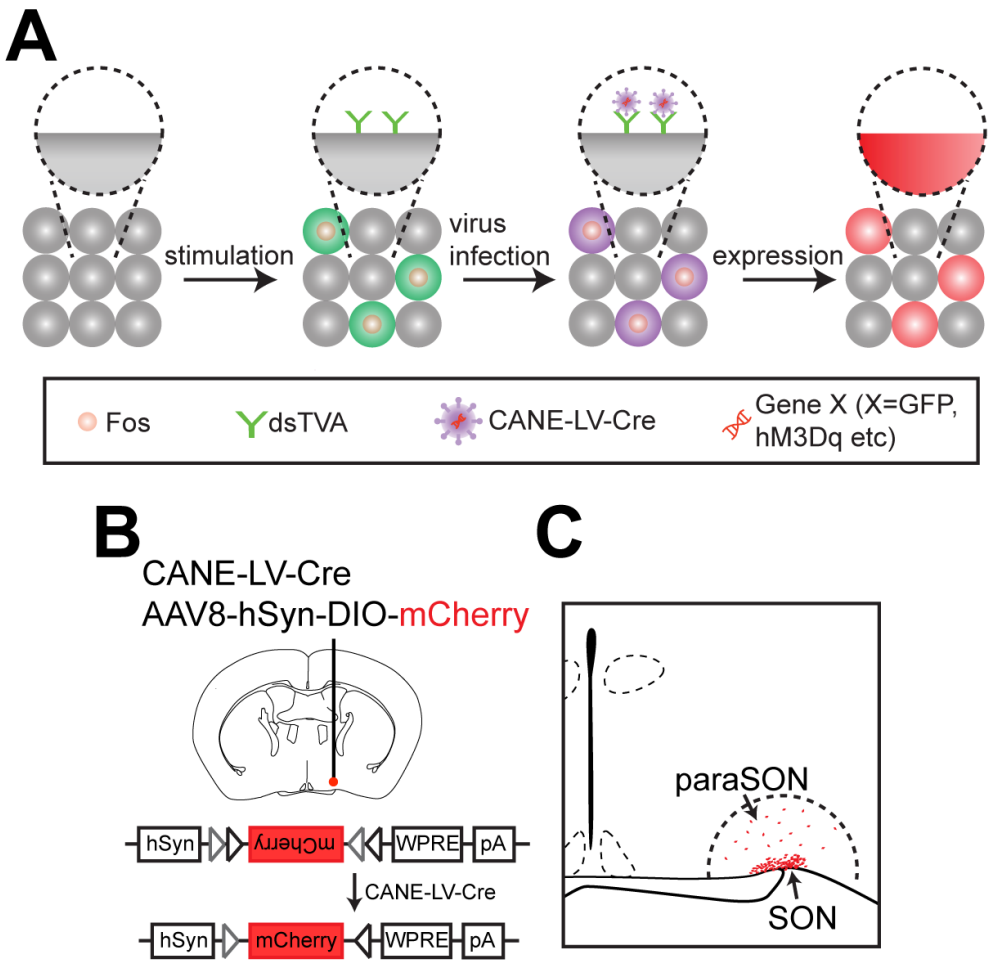

Figure 8. Capturing AAN with CANE technology.
(A) Schematic diagram of CANE technology.
(B) Viral construct and injection site in Fos^{TVA} mice.
(C) Illustration of the SON and paraSON. paraSON is defined as a region within 500 ◎m radius circle with the up-corner of the optic chiasm/tract as the center, extending from anterior to posterior hypothalamus.

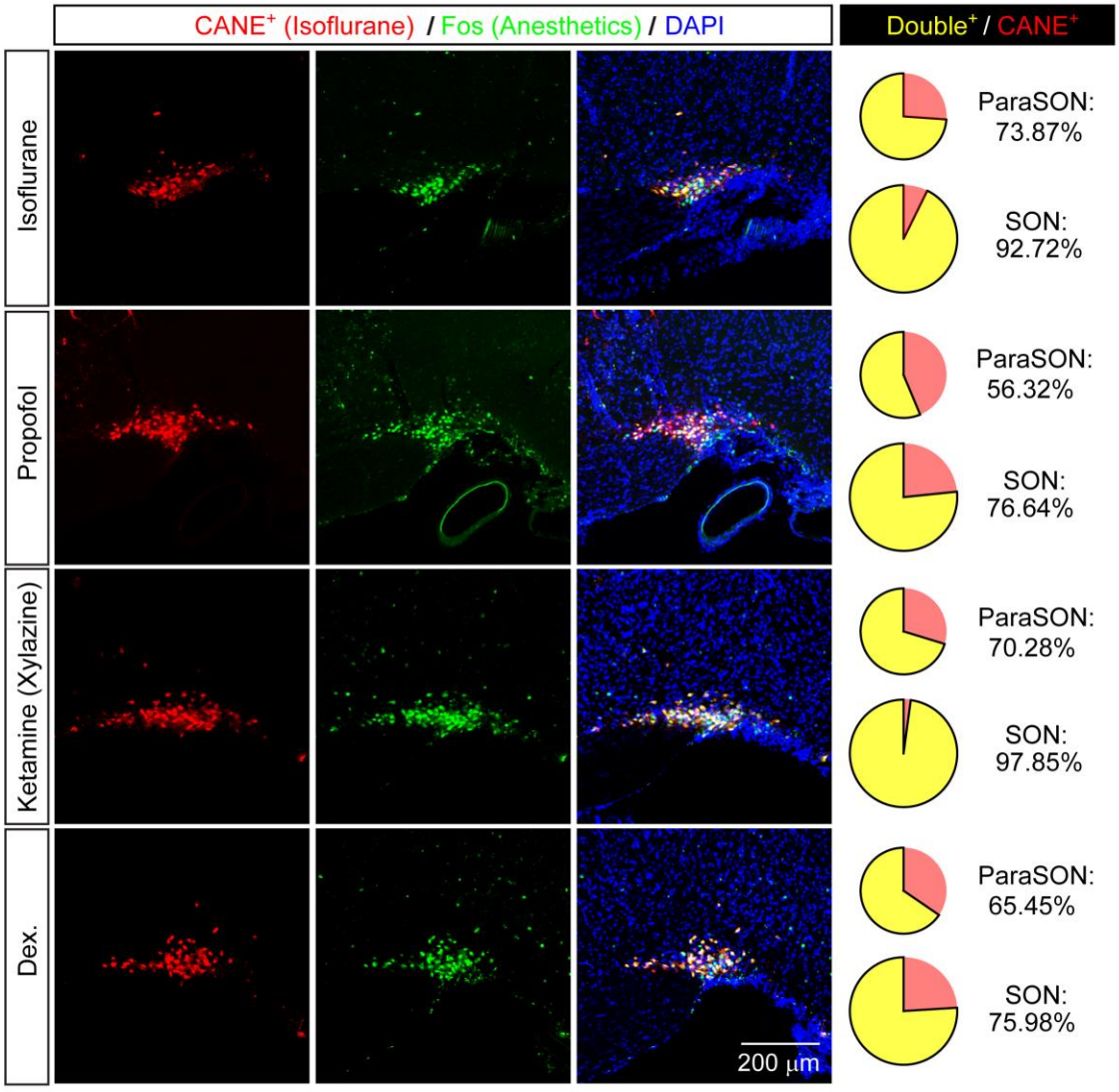
CANE+ (Isoflurane) / Fos (Anesthetics) / DAPI
Double+ / CANE+
Isoflurane
Propofol
Ketamine (Xylazine)
Dex.
ParaSON:
73.87%
SON:
92.72%
ParaSON:
56.32%
SON:
76.64%
ParaSON:
70.28%
SON:
97.85%
ParaSON:
65.45%
SON:
75.98%
200 μm

Figure 9. A shared neuronal population is activated by different anesthetics.
Left panels, representative images of CANE-captured isoflurane-activated neurons (red) and Fos+ neurons (green) induced by re-exposure to either isoflurane again, or to Propofol, Ketamine (plus xylazine), or dexmedetomidine (Dex). Right panels, pie charts showing the percentage of initial CANE-captured isoflurane-activated neurons that are re-activated (Fos+) by different anesthetics in SON as well as in paraSON. Neurons were from 7-30 slices from 2-4 mice for each condition.

3.2 Multiple GA drugs activated a shared AAN ensemble

After validation of CANE technology in capturing AAN ensemble, we immediately realized the CANE-capturing of AAN also afforded us the unique opportunity to investigate whether isoflurane activated AAN can also be activated by other distinct GA drugs. To achieve this goal, we first utilized CANE technology to specifically transduce mCherry in isoflurane-activated AAN, and a month later, we subjected these mice to treatments of other widely used general anesthetics in research and clinical settings, including Propofol, Ketamine (with or without Xylazine), or dexmedetomidine (Dex), followed by Fos staining to visualize the activated neurons with green color (Franks, 2008) (Figure 9). Interestingly, Propofol, Ketamine (plus Xylazine), and Dex all re-activated a large population of AAN that were previously activated by isoflurane in both SON and paraSON region (Figure 9. In SON, 76.64%, 97.85%, and 75.98% Isoflurane-mCherry$^+$ cells were Fos$^+$ under Propofol, Ketamine, and Dex respectively; in paraSON, 56.32%, 70.28%, and 65.45% isoflurane-mCherry$^+$ cells were Fos$^+$ under Propofol, Ketamine (plus Xylazine), and Dex, respectively). In addition, Ketamine alone also reactivated a shared population of AAN, albeit to a lesser extent (Figure 10. In SON, 72.69% isoflurane- mCherry$^+$ cells were Fos$^+$; in paraSON, 44.36% isoflurane-mCherry$^+$ cells were Fos$^+$ under Ketamine only condition). Our results demonstrated the AAN we discovered here represent a common neural substrate between multiple distinct GA drugs.

Instead of using neural activity marker Fos, we also decided to gather a more direct evidence of neural activation with ex vivo electrophysiology. AAN was first labeled with mCherry through the help of CANE technology. We then could perform whole-cell patch-clamp recording on specific CANE-mCherry captured neurons guided by red fluorescent under the microscope. By infusion of GA drugs into the recording chamber, we discovered that isoflurane, Propofol, Ketamine, and Dex all significantly depolarized the membrane potentials of AAN (Figures 11, $\Delta V = 11.38 \pm 1.82$ mV induced by isoflurane, n = 11; $\Delta V = 5.10 \pm 0.98$ mV induced by Propofol, n = 32; $\Delta V = 7.09 \pm 1.89$ mV induced by Ketamine, n = 25; $\Delta V = 12.95 \pm 1.79$ mV induced by Dex, n = 27 recorded AAN), consistent with the fact that these cells became Fos^+ in vivo under GA. Taken together, with Fos staining and ex vivo brain slice recording, our results strongly support the idea that these hypothalamic AAN represent a common neural substrate activated by distinct classes of GA drugs.

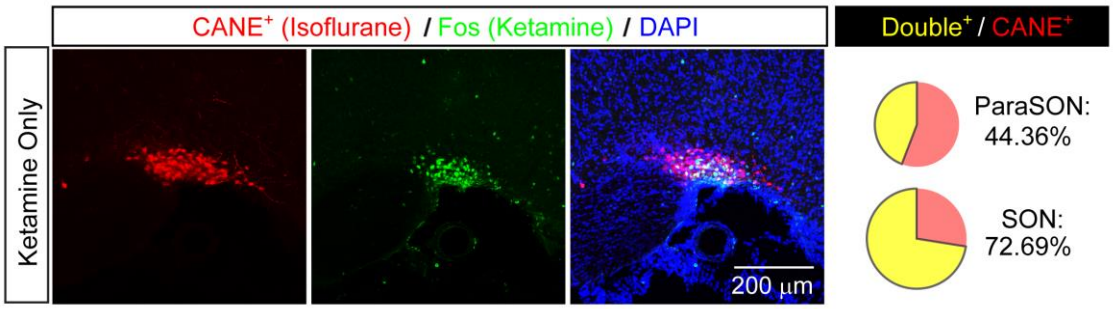

Figure 10. Ketamine alone also induce Fos expression in AAN.
Left panels, representative images of CANE-captured isoflurane-activated neurons (red) and Fos$^+$ neurons (green) induced by Ketamine treatment only. Right panels, pie charts showing the percentage of initial CANE-captured isoflurane-activated neurons that are re-activated (Fos$^+$) by Ketamine. 7-21 slices for each region from 2 mice.

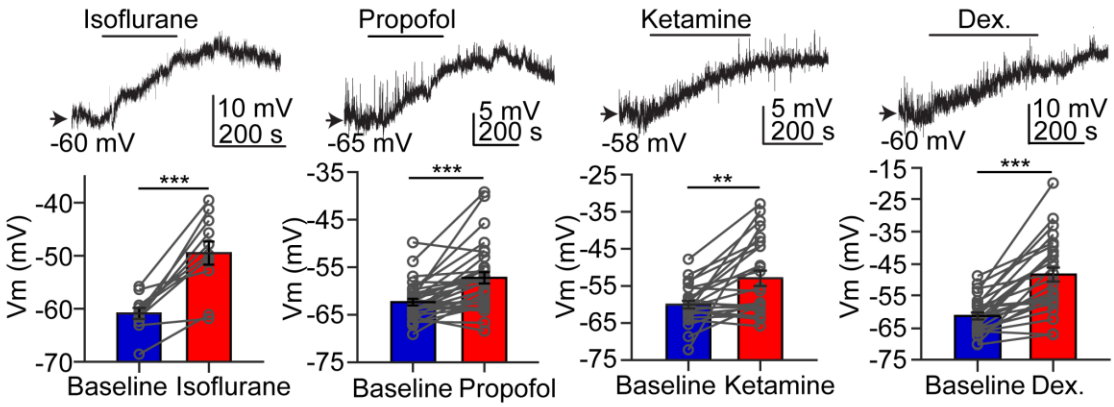

Figure 11. Whole-cell patch-clamp recording of CANE-captured isoflurane-activated neurons in acute brain slices following treatments of different classes of anesthetics. Top, representative membrane potential changes after the application of drugs; bottom, statistical summary for all recorded neurons. n = 11 neurons for isoflurane; n = 32 for Propofol; n = 25 for Ketamine; n = 27 for Dex. Wilcoxon signed-rank tests for all drugs. Data are presented as mean ± s.e.m. **P < 0.01, ***P < 0.001.

4. Activation of AANs promotes slow-wave sleep and extends general anesthesia

4.1 Chemogenetic activation of AAN strongly enhances SWS

One of the most intriguing questions that we could imagine is what would happen if we artificially stimulate AAN. Do we able to change the brain state of mice by just activating this small population of neurons? Since the entire population of AAN (SON plus paraSON) are distributed from ventral preoptic regions to the most posterior end of SON (more than 1.2 mm along the anterior-posterior axis in the ventral edge of hypothalamus), we utilized chemogenetics (Roth, 2016) to activate this spatially extended population of neurons. Chemogenetics has two major components, (1) an engineered G protein-coupled receptor hM3Dq (modified from human M3 muscarinic receptor), which presumably only activated by (2) exogenous synthetic ligands Clozapine N-oxide (CNO). However, there is a report recently indicated that CNO can convert into clozapine in vivo which highlights the importance of incorporating a proper drug control group to rule out off-targets of the CNO itself (Gomez et al., 2017).

Through CANE technology, chemogenetic activator hM3Dq (AAN-hM3Dq) or control mCherry (AAN-mCherry) was expressed in AAN by co-injecting CANE-LV-Cre and Cre-dependent hM3Dq (Figures 12). First, as a proof of principle, we try to validate the functionality of hM3Dq expressing on AAN ensemble. By performing ex vivo electrophysiology in acute brain slices, we discovered that application of Clozapine-N-Oxide (CNO), the ligand for hM3Dq, induced a persistent firing mode of hM3Dq-

expressing AAN (Figure 12C). Furthermore, systemic intraperitoneal injection of CNO in animals also resulted in robust Fos expression in AAN-hM3Dq cells (Figure 12B). To examine the in vivo effects on brain states, we injected AAN-hM3Dq or control AAN-mCherry mice with either CNO or saline while simultaneously recorded their brain state with EEG from frontal and parietal cortex and EMG from the bilateral neck muscles for two hours immediately after drug treatments (during dark phase, 9~11 pm, when the internal sleep drive is minimal) (Figure 13).

In the baseline condition during the early dark phase, such as saline injected AAN-hM3Dq, as well as saline or CNO injected AAN-mCherry control mice, we could observe normal interspersed wakefulness signified by high-frequency oscillation and lots of muscle activity, short bouts of SWS characterized by higher power oscillations at delta (1-4 Hz) frequency and low EMG activity, and occasional episodes of REM sleep characterized by elevated and regular theta oscillation (6~10 Hz) with very low amplitude of EMG (Scammell et al., 2017; Weber and Dan, 2016) (Figures 13A-B). Strikingly, artificially activate the AAN through CNO treatment in AAN-hM3Dq mice, the total duration of SWS (a naturally occurring unconscious state) nearly doubled than that of three control groups, and the average total wake time was concomitantly reduced in half (Figures 13A-B, on average 56.53 ± 3.70% of time SWS for hM3Dq-CNO, versus 28.30 ± 2.71%, 23.86 ± 2.36%, 24.83 ± 1.05% for hM3Dq-saline, mCherry-saline, mCherry-CNO conditions, respectively), while there was no pronounce effect in REM sleep.

We further performed more analysis on the detailed parameters of SWS, Wake, and REM sleep. It turned out the SWS-promoting effect of chemogenetic activation of AAN was primarily attributable to extending the average SWS bout duration (Figure 13C, average 48.01 ± 4.85 sec per SWS bout for hM3Dq-CNO, versus 26.95 ± 3.50, 24.52 ± 3.10, 27.35 ± 3.26 sec for hM3Dq-saline, mCherry-saline, mCherry-CNO conditions, respectively, during dark phase with 4-s scoring window). In other words, once we activated AAN, the mice sleep much longer but does not alter their sleep frequency. This result suggests that, instead of acting as a neuronal switch for brain states, AAN works more like a sleep stabilizer. This biological property is likely mediated by slow, long-lasting, and systematic effects mediated by neuropeptides or hormonal signals.

Furthermore, we were very curious about whether the SWS induced by AAN activation is qualitatively identical to natural occurring SWS. To answer this question, we decided to perform exquisite spectral analyses on frontal and parietal EEG traces that would isolate subtle oscillation differences. We discovered that the power-frequency curves of SWS under AAN-activation almost completely overlapped with those of the naturally occurring SWS with the peak power at delta wave both in frontal and parietal EEGs (Figures 14-15). Also, the power-frequency curves of wakefulness and REM sleep were also identical (Figures 14-15). In sum, our data strongly suggests that AAN identified here likely represent the shared neural pathway between different GA drugs

and natural sleep since activating AAN alone is sufficient to promote and extend the duration of SWS.

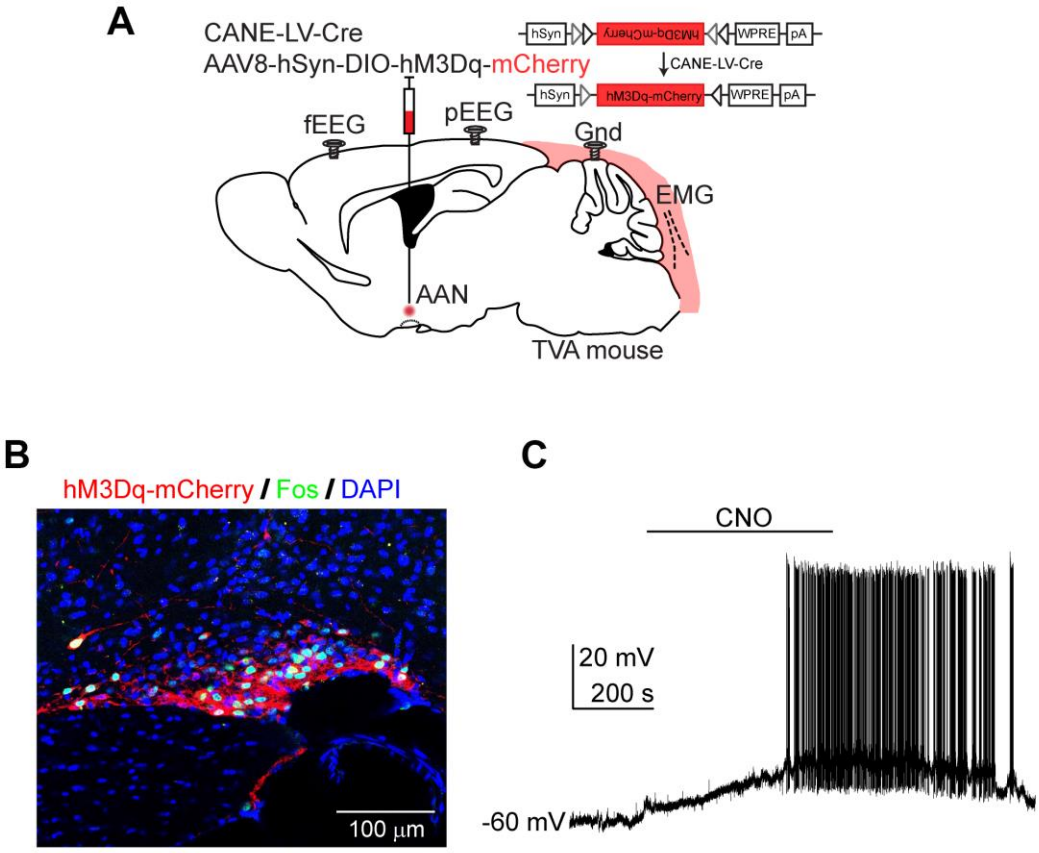

Figure 12. Expressing chemogenetic actuator in AAN.
(A) Viral-genetic strategy for expressing hM3Dq-mCherry in AAN, and the layout of EEG/EMG recording. fEEG, frontal EEG; pEEG, parietal EEG; Gnd, ground.
(B) Systemic CNO treatment (intraperitoneal injection) induced robust Fos (green) expression in the hM3Dq-mCherry+ (red) neurons.
(C) Depolarization of hM3Dq-mCherry+ neurons by CNO in acute brain slice.

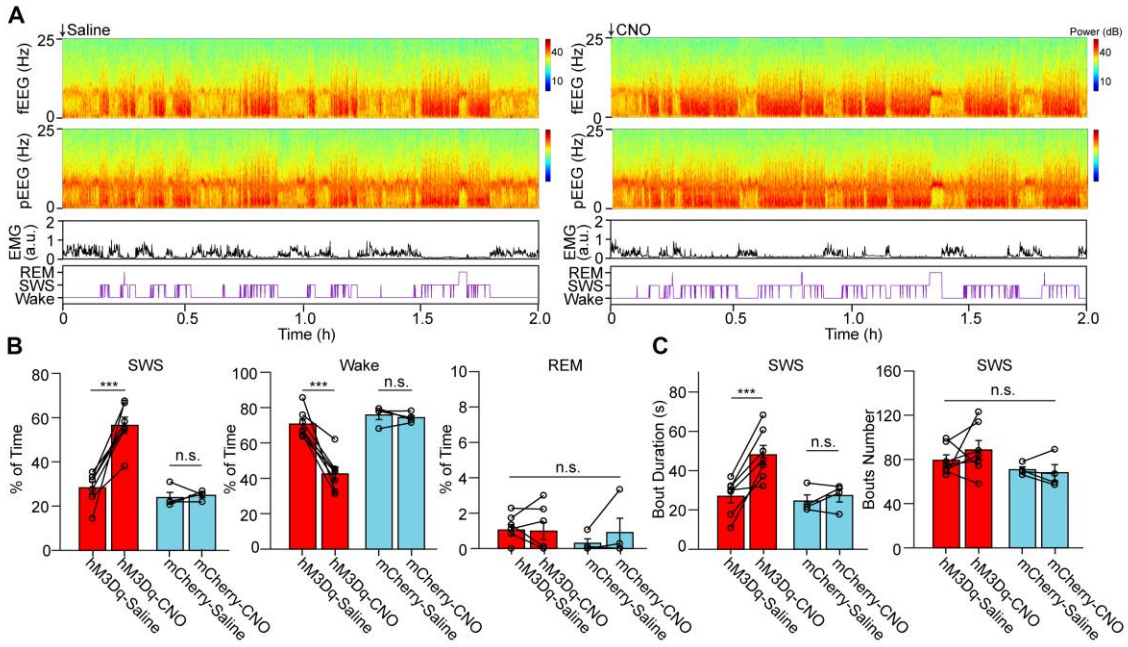

Figure 13. Chemogenetic activation of AAN significantly potentiates SWS.
(A) Representative polysomnographic recording following either saline or CNO treatment in AAN-hM3Dq mouse. Top two panels, representative spectrogram from fEEG and pEEG; third, EMG; bottom, brain state annotated. SWS, slow-wave sleep; REM, rapid-eye movement sleep. (B) Percentage of time spent in SWS, Wake and REM across 2 hours after injection. Two-way repeated measures ANOVA followed by Sidak's post hoc test. n = 7 mice for hM3Dq-mCherry and n = 4 mice for mCherry group.
(C) Bout duration and number of SWS across 2 hours after injection. Two-way repeated measures ANOVA followed by Sidak's post hoc test. n = 7 mice for hM3Dq and n = 4 mice for mCherry group. Data are presented as mean ± s.e.m. ***P < 0.001.

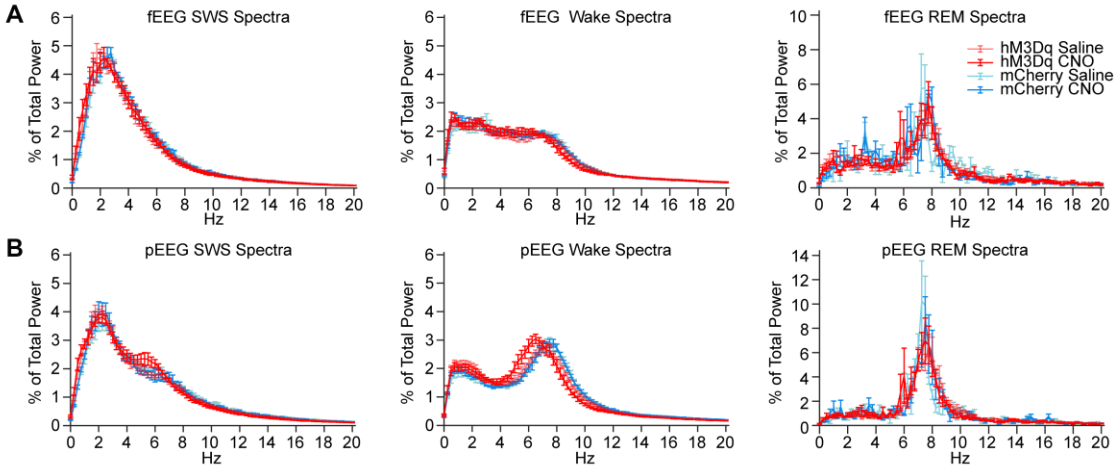

Figure 14. Power-frequency analysis across SWS, Wake, and REM from different experimental groups. n = 7 mice for hM3Dq and n = 4 mice for mCherry group.

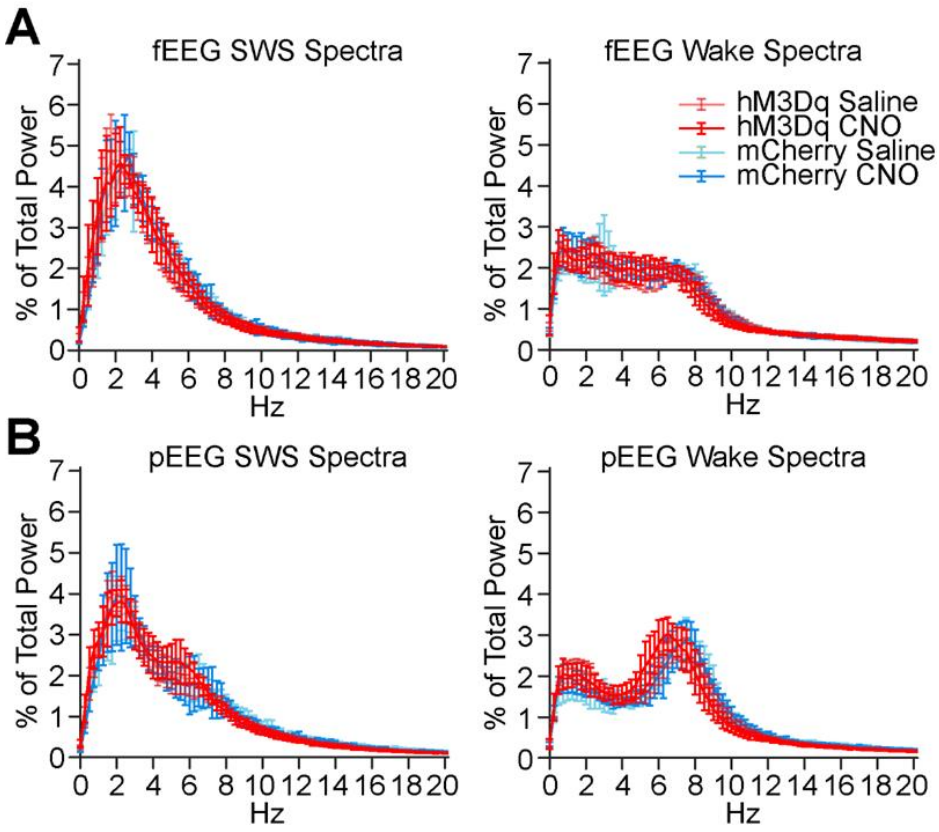

Figure S15. Power spectra of SWS and Wake plotted with 95% confidence interval.
(A-B) Power-frequency analysis of frontal (A) and parietal (B) EEG during SWS and Wake states for hM3Dq and mCherry groups following either saline or CNO treatment. fEEG, frontal EEG; pEEG, parietal EEG. n = 7 mice for hM3Dq and n = 4 mice for mCherry group.
Data are presented as mean ± 95% confidence interval.

4.2 Chemogenetic activation of SON AAN alone enhances SWS

The majority of cells among AAN that we discovered were previously unsuspected SON neurons, which, according to the previous literature, are neuroendocrine cells. These cells have extensive axons traveled across blood-brain barrier (BBB) to innervate posterior pituitary, where hormones are released into general circulation. Since their axons are not protected by BBB, we would retrogradely label these cells by systematically inject Fluorogold tracer (Weiss and Cobbett, 1992). It turned out a huge fraction of AAN could be labelled with Fluorogold (97.40% of SON AAN is fluorogold$^+$, while 8.18 % of paraSON AAN is fluorogold$^+$, thus identified as neuroendocrine cells (Figure 16).

Next, we want to determine whether activating a specific group of SON cells alone is sufficient to increase SWS. While there is no available Cre-driver line that expresses in all SON-AAN, we decided to utilize AVP$^{Cre/+}$ mice since ~85% of SON-AAN are AVP$^+$ cells (which also co-express Pdyn (Watson et al., 1982)), but keeping in mind the caveat that AVP^{Cre} mice are homozygous lethal (our observation), the knock-in construct very likely disrupts endogenous cellular functions. We could not use Pdyn^{Cre} mice since there are many Pdyn$^+$ neurons in paraSON region that are not activated during GA.

To manipulate SON AVP$^+$ cells, we stereotaxically injected Cre-dependent AAV-DIO-hM3Dq bilaterally into SON region of heterozygous AVP$^{Cre/+}$ mice, and further

implanted frontal and parietal EEGs and EMG electrodes in the same mice. We discovered chemogenetic activation of SON AVP$^+$ neurons alone was indeed sufficient to potentiate SWS (Figure 17, 27.74 ± 1.89% and 46.87 ± 2.11% of time spent in SWS for saline and CNO conditions), although the quantity of SWS increase was much less than that induced by activating all AAN with the help of CANE technology (99.75% SWS increase for activating all AAN versus 68.96% for activating SON AVP$^+$ neurons). Even though, our results still reveal a previously under-appreciated role of vasopressin$^+$/ dynorphin$^+$ SON neuroendocrine cells in promoting SWS.

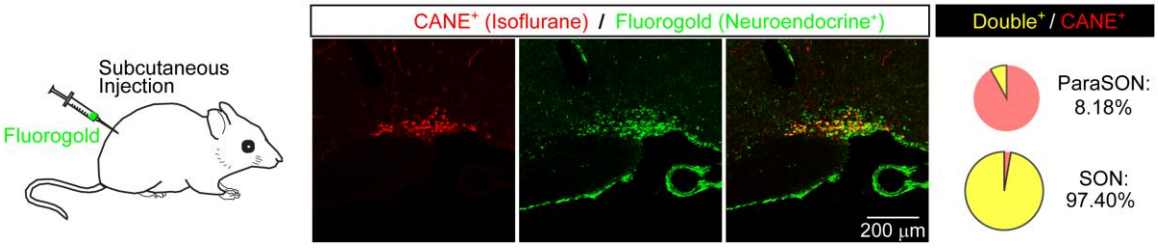

Figure 16. Hypothalamic AAN are neuroendocrine cells.
Left, 5% Fluorogold (pseudocolor as green) was subcutaneously injected into AAN-mCherry mouse. Five days later, Fluorogold would be fully up-taken by neuroendocrine cells through the general circulation. Middle, representative colocalization image of AAN (mCherry) and neuroendocrine cells (green). Right, percentage of AAN colocalized with Fluorogold+ cells. 15-25 slices for each region from 2 animals.

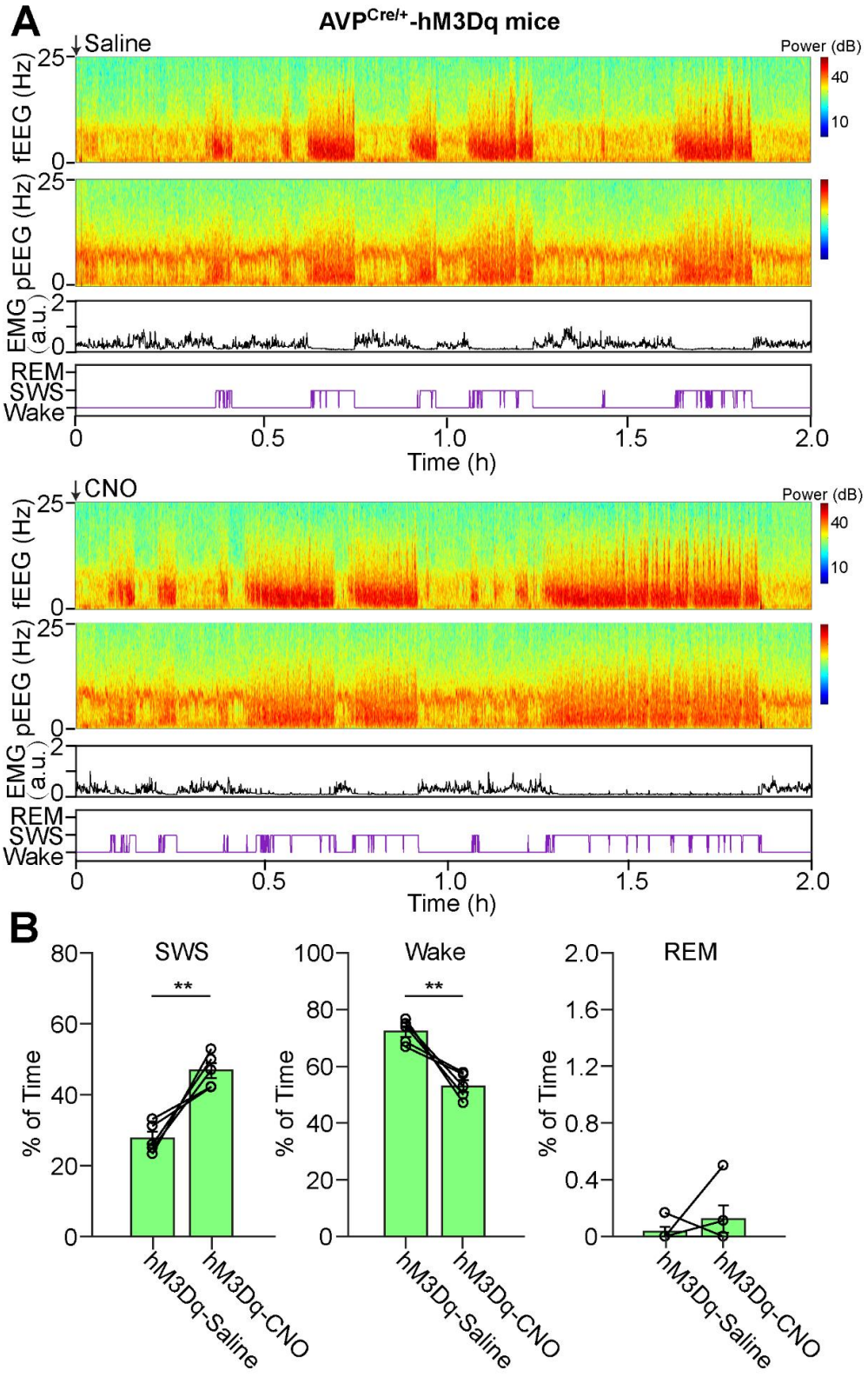
A
AVP^Cre/+-hM3Dq mice
Saline
CNO
Power (dB)
40
10
fEEG (Hz)
pEEG (Hz)
EMG (a.u.)
REM
SWS
Wake
Time (h)
B
SWS
Wake
REM
% of Time
**
hM3Dq-Saline
hM3Dq-CNO

Figure 17. Chemogenetic activation of SON AVP neurons potentiate SWS sleep.
(A) Representative EEG/EMG recording following either saline (top) or CNO (bottom) injection. (B) Percentage of time spent on SWS, Wake and REM across 2 hours after saline or CNO injection. n = 5 mice. Paired-t test.
Data are presented as mean ± s.e.m., **P < 0.01.

4.3 Brief optogenetic activation of AAN promotes subsequent sleep

Since AAN includes a particular large proportion of neuroendocrine cells in SON, which are able to secrete huge quantities of neuropeptides into the cerebrospinal fluid through somatodendritic release, as well as release large amount of hormones through axon terminals in the posterior pituitary (Ludwig and Leng, 2006). Considering that peptides and hormones signaling generally lasts much longer than classic fast neurotransmitters, such as glutamate and GABA, we therefore want to test whether a brief stimulation of AAN is sufficient to promote and sustain subsequent sleep. To have a better temporal control of AAN activity, we decide to utilize optogenetics (Boyden et al., 2005; Yizhar et al., 2011) which is able to control the neuronal action potential in milli-second time-scale with pulses of light.

We expressed the light-activated cation channel channelrhodopsin 2 (AAN-ChR2) or control GFP (AAN-GFP) in AAN with CANE technology, followed by implantation of fiber optics (200 um, NA : 0.39, Thorlabs, Inc.) bilaterally above the AAN ensemble (Figures 18A). With ex vivo whole-cell patch-clamp electrophysiology recording, we validated that blue-light (10 Hz, 10 ms for each pulse) indeed drove reliable and temporally precise neuronal spikes of labeled AAN in acute brain slices (Figures 18B). For in vivo behavioral experiments, we first performed photo-stimulation in control AAN-GFP mice. To our surprise, we discovered that blue laser (473-nm) stimulation itself (10 Hz, 10 ms/pulse, 1-s ON and 1-s OFF, 3~5mW, for total of 3 min) had a

significant arousal effect on control AAN-GFP animals during the Laser-On period (Figures 18C-D). Since the optic fibers were implanted bilaterally closely above AAN regions which are located immediately dorsal to optic chiasm and optic tracts, we reasoned that such deep brain photo-illumination might activate melanopsin-expressing retinal ganglion cells thus promote wakefulness. Indeed, a previous study did confirm our speculation (Danskin et al., 2015). With simultaneous electrophysiological recordings in mouse retinal, they clearly demonstrated that optogenetic deep brain illumination resulted in retinal cells activation, and the effects are even more pronounce with yellow or red light stimulation.

Remarkably, despite the artifact of light-induced arousal, the same 3 min of laser stimulation in AAN-ChR2 mice, which would definitely activate AAN, drastically increased SWS in the post-stimulation period signified by a dominant delta oscillation (1-4 Hz) and minimal muscle activity. Strikingly, the sleep-promoting effect could last more than 10 minutes after we turned off the laser (Figures 18C-D). This result indicated that a brief optogenetic activation of AAN is sufficient to exert a long-lasting effect on the global brain state. In the meanwhile, we also observed a complementary decrease in wake time, while there was no significant difference in REM during the post-stimulation period in AAN-ChR2 mice (Figures 18C-D). These results are nicely accordance with our previous chemogenetic experiment.

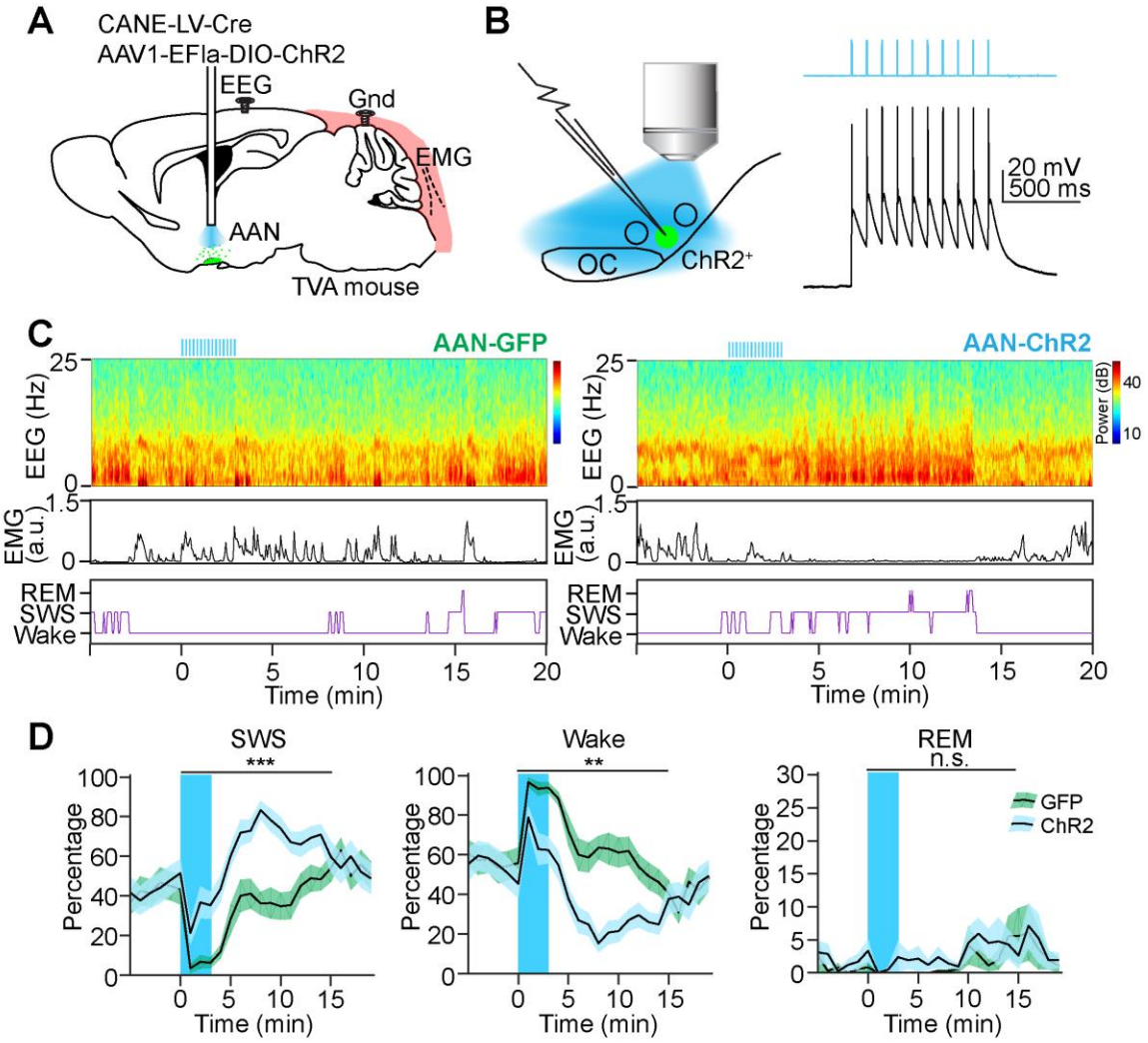
A
CANE-LV-Cre
AAV1-EFla-DIO-ChR2
EEG
Gnd
EMG
AAN
TVA mouse
B
OC
ChR2+
20 mV
500 ms
C
AAN-GFP
AAN-ChR2
EEG (Hz)
Power (dB)
EMG (a.u.)
REM
SWS
Wake
Time (min)
D
SWS
Wake
REM
n.s.
Percentage
GFP
ChR2
Time (min)

Figure 18. Brief Optogenetic activation of AAN promotes subsequent SWS.
(A) Viral-genetic strategy for expressing ChR2 in AAN, the layout of optic fiber implantation, and EEG / EMG recording. Gnd, ground.
(B) Blue laser evokes reliable neuronal spikes in ChR2+ AAN.
(C) Representative polysomnographic recording of AAN-GFP (left panel) and AAN-ChR2 (right panel) mice before, during, and after laser stimulation (10 Hz, 10 ms pulses, 1s-On and 1s-OFF, 3 min, 3~4 mW measured at the fiber tips). Top, representative spectrogram of EEG; middle, EMG; bottom, brain state annotated.
(D) Percentage of time spent in SWS (left), Wake (middle), and REM (right) before, during, and after the period of laser stimulation (blue shaded area). n = 28 trials from 5 ChR2 mice (4~6 trials per mouse); n = 24 trials from 4 GFP mice (6 trials per mouse). Permutation test were performed across two groups. Data are presented as mean ± s.e.m. **P < 0.01, ***P < 0.001.

4.4 Brief optogenetic activation of AAN extends general anesthesia

The optogenetic effect of AAN on promoting SWS is very intriguing to us. However, since AAN is activated during GA, we were very curious about whether activation of AAN could have any effect on the brain state during GA. With the help of CANE technology, light-activated cation channel channelrhodopsin 2 (ChR2) or control GFP is specifically expressed in AAN. Volatile anesthetics Isoflurane (1%) was infused immediately after photo-illumination (10 Hz, 10 ms/pulse, 1-s ON and 1-s OFF, 3-5 mW, for total of 3 minutes), the brain states of animals were determined by EEG and EMG recording. Through EEG spectrogram and EMG activity, we could reliably and precisely specify the time of induction and emergence of GA. The induction of GA is characterized by enhanced slow and ultra-slow (0~1 Hz) wave activities, and the muscle activity is much reduced; while the emergence of GA is signified by re-gaining of muscle activity and diminished low frequency oscillation in EEG.

Very surprisingly, we discovered that photo-activation of AAN did not alter the time of GA induction, but significantly delayed the emergence from GA. In other words, animals would stay longer under GA once we activated AAN (Figure 19). Again, these results suggest that, instead of using fast neurotransmitters, AAN adopts slow and long-lasting peptidergic or hormonal signaling in sustaining a global sedative state.

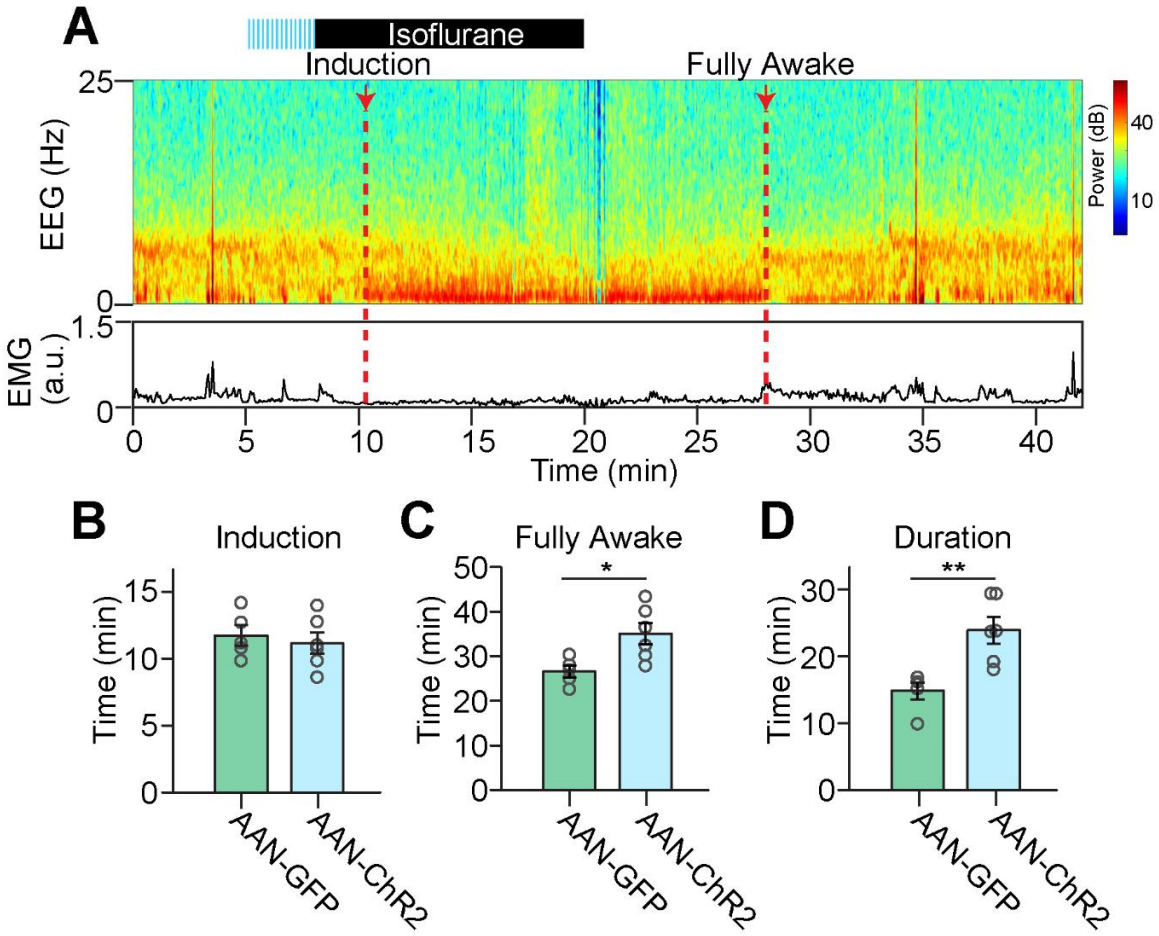
A
Isoflurane
Induction
Fully Awake
25
0
EEG (Hz)
Power (dB)
40
10
1.5
0
EMG (a.u.)
0
5
10
15
20
25
30
35
40
Time (min)
B
Induction
Time (min)
15
10
5
0
AAN-GFP
AAN-ChR2
C
Fully Awake
*
50
40
30
20
10
0
Time (min)
AAN-GFP
AAN-ChR2
D
Duration
**
30
20
10
0
Time (min)
AAN-GFP
AAN-ChR2

Figure 19. Optogenetic activation of AAN prolongs the duration of GA.
(A) Representative EEG/EMG recording across experimental session. Top, representative spectrogram of EEG; bottom, EMG. Isoflurane (1%) was infused immediately after laser stimulation (10 Hz, 10 ms pulses, 1s-On and 1s-OFF, 3 min, 3~4 mW measured at the fiber tips). Induction time is determined by appearance of slow oscillation and reduction of movement. Fully awake time is determined by reduction in slow-wave power and elevated muscle activity continuously for more than 1 min.
(B-D) Statistical analysis of Induction time (B), fully awake time (C), and anesthesia duration (D). n = 5 for AAN-GFP mice, n = 6 for AAN-ChR2 mice. Two-sample t-test. Data are presented as mean ± s.e.m., *P < 0.05. **P < 0.01.

4.5 AAN is activated by sleep pressure

With state-of-the-art chemogenetics and optogenetics toolkits, we demonstrated that artificial activation of AAN largely potentiated SWS by extending bout duration. The key question remains is the online neural activity of AAN during natural sleep. One strategy that we could do is to place the animals under consolidated sleep for two-hour, then stained the activated neurons with Fos. However, rodents typically do not have stable sleep. Although they spend a large portion of time in sleep during the light phase, their sleep pattern is actually very fragmented (Weber and Dan, 2016). To make mice sleep longer, we usually have to slightly deprive their sleep in advance (Anaclet et al., 2012).

With CANE technology, AAN were first labelled with mCherry in a cohort of mice (Figure 20). Subsequently, these mice were randomly assigned into three experimental groups: (1) first group stayed in home cage without any disturbance, (2) second group undergone sleep deprivation for 5 hours, and (3) third group undergone sleep deprivation for 5 hours followed by recovery sleep for 2 hours. Afterwards, their brains were collected for Fos staining (Figure 20B). To sleep deprive the animals, we followed a relatively mild and stress-free protocol as previously described (Anaclet et al., 2012; Chung et al., 2017) by constantly introducing novel objects to the animals every 20~30 minutes in their home cage.

Interestingly, although we discovered recovery sleep (RS) group slightly recruited

more AANs than home cage (HC) control, we realized it was sleep deprivation (SD) that strongly activated AANs. After recovery sleep, the Fos expression in AAN gradually returned to baseline (Figure 20C-D). These results suggest that, instead of sleep behavior itself, it is the craving for sleep (sleep pressure) that drives the activation of these neurons. This surprisingly result may explain why sleep deprivation can potentiate subsequent GA (Tung et al., 2002). Our finding also dovetails nicely with our chemogenetic and optogenetic experiment results in that activation of AAN can promote subsequent SWS.

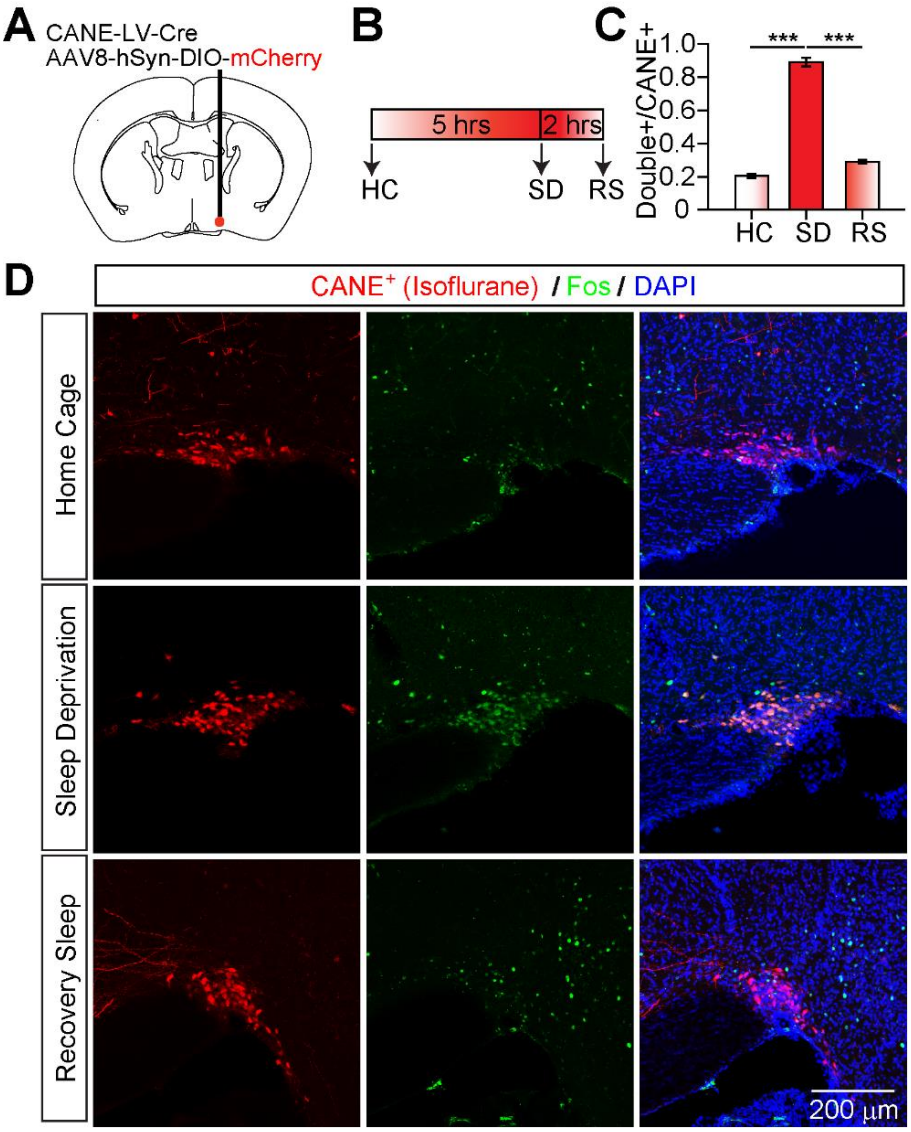

Figure 20. AAN is activated by sleep pressure

(A) CANE strategy for specifically expressing mCherry in AAN.

(B) Time windows for each experimental group. HC, home cage; SD, sleep deprivation; RS, recovery sleep.

(C) Total percentage of CANE-captured neurons reactivated under HC, SD, and RS. One-way ANOVA followed by Sidak's post hoc test. n = 3 mice for HC, n = 4 for SD, n = 3 for RS.

(D) Representative Fos staining from HC, SD, and RS.

Data are presented as mean ± s.e.m. ***P < 0.001.

5. Inhibition of AANs shortens general anesthesia and disrupts natural sleep

5.1 Ablation of AAN disrupts natural sleep

After the successful demonstrating the gain-of-function effects on sleep and GA by activating AAN through chemogenetics and optogenetics, a following question is whether inhibition or ablation of AAN impact natural sleep or GA. To test this hypothesis, we utilized a potent genetic strategy to achieve targeted-cell-type ablation through selectively expressing diphtheria toxin receptor (DTR) (Saito et al., 2001). With CANE technology, DTR (AAN-DTR) or control mCherry (AAN-mCherry) was specifically expressed in AAN ensemble, and their sleep-wake patterns were monitored with polysomnography recording (Figure 21-23). By the time of diphtheria toxin (DT) injection, only the neurons that expressed DTR would be ablated, while the rest of nearby neurons would not be affected.

We performed chronic EEG and EMG recordings (whole day) before and after diphtheria toxin (DT) injection, which would induce ablation of AAN that expressed DTR (Figure 21B). In the AAN-DTR group, over the course of two weeks post DT injection, the total duration of both SWS and REM sleep in the mice gradually and substantially declined compare to the baseline condition (Figure 22, n = 9 mice, SWS: 39.09 ± 0.97, 38.34 ±1.23, 37.69 ± 1.94, 26.55 ± 2.30, 22.42 ± 3.19% of time; REM: 5.46 ± 0.41 , 5.62 ± 0.43, 2.60 ± 0.43, 1.59 ± 0.39, 1.85 ± 0.49% of time at baseline, day 2, 5, 1-week, or 2-week post DT, respectively), while these effects were not observed in DT treated AAN-

mCherry mice (Figure 23) in which AAN did not express DTR.

Interestingly, we discovered the effect on SWS is largely due to shortened bout duration (but not the total bout numbers), indicating ablating AAN caused the inability to sustain SWS, while the bout number was largely unaffected (Figure 22, average SWS bout duration: 100.23 ± 7.82, 83.24 ± 5.75, 77.34 ± 7.20, 56.93 ± 8.28, 43.94 ± 6.33 sec at baseline, day 2, 5, 1-week, or 2-week post DT, respectively, averaged across the whole day recording with 10-s scoring window). On the other hand, the reduction in REM sleep is mainly attributable to reduced bout numbers, suggesting that the AAN-DTR mice had a difficulty in entering REM sleep, while the bout duration was unchanged (Figure 22, average REM bout number: 86.89 ± 4.97, 102.00 ± 9.16, 42.56 ± 9.83, 26.56 ± 6.88, 32.11 ± 8.57 number of bouts at baseline, day 2, 5, 1-week, or 2-week post DT, respectively). Since the REM sleep typically occurs after a long and consolidated SWS, we reasoned the effect on REM sleep may be caused by fragmented SWS in advance. Importantly, these effects were not present in AAN-mCherry mice after DT injection (Figure 23).

Furthermore, we noticed that the delta (1~4 Hz) power of SWS and the theta (6~10 Hz) power of REM sleep were gradually and strikingly declined in AAN-DTR mice after the treatment of DA, suggesting that neuronal oscillations which are signatures of normal sleep were severely impaired (Figures 22, right most panels). One third of animals (3 out of 9 mice) eventually died at the end of experimental session (~ 3 weeks)

presumably due to severe sleep deprivation. We had to terminate the experiments and sacrifice the animal in advance since most of them were very sick. The time course of their mortality closely matches that of previous reports (Everson et al., 1989). Again, none of these adverse effects were observed in DT treated AAN-mCherry mice (Figure 23). Together, our results indicated that AAN are also very essential for promoting and stabilizing both SWS and REM sleep.

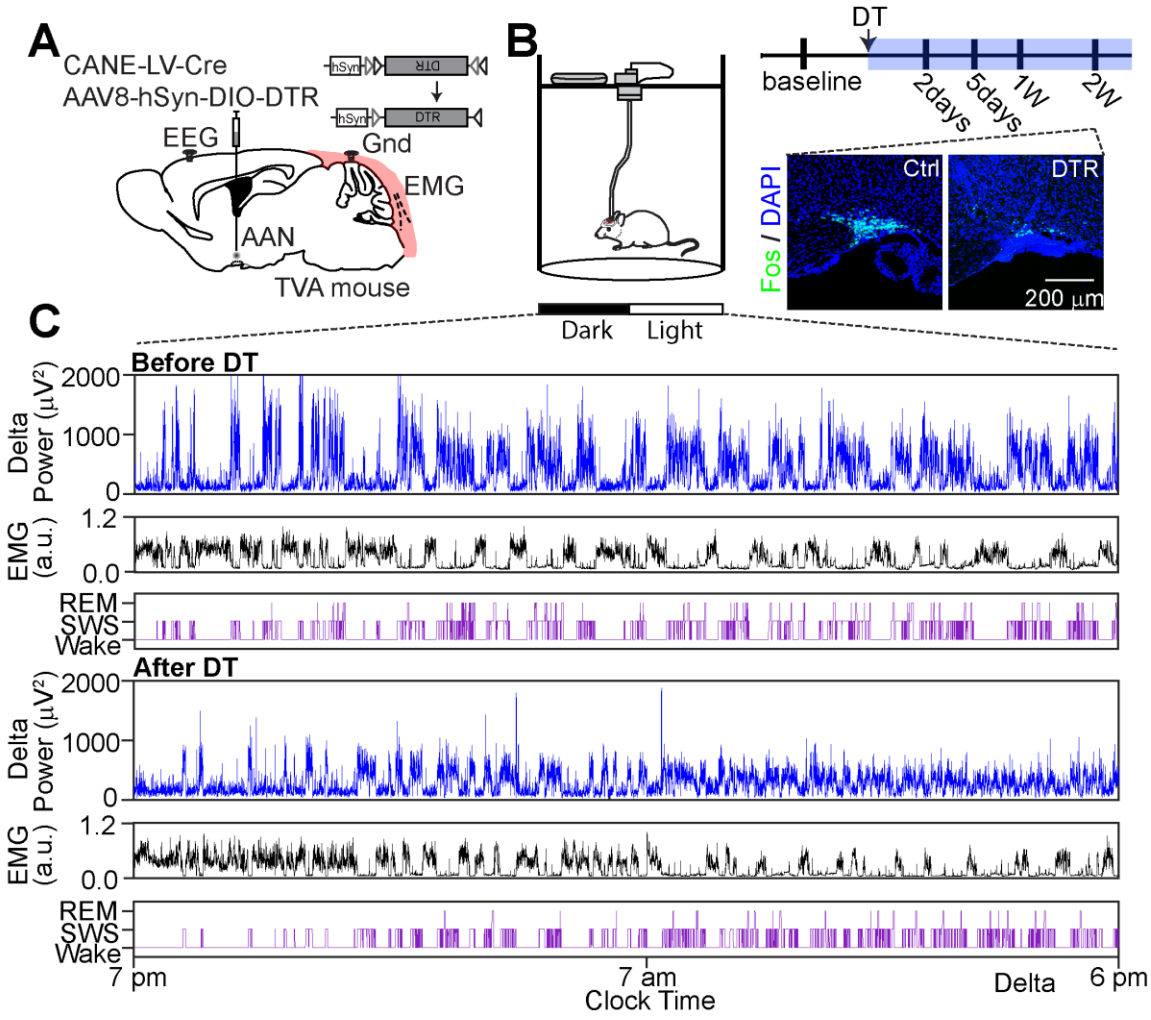
A
CANE-LV-Cre
AAV8-hSyn-DIO-DTR
hSyn
DTR
EEG
Gnd
EMG
AAN
TVA mouse
B
DT
baseline
2days
5days
1W
2W
Ctrl
DTR
Fos / DAPI
200 μm
Dark
Light
C
Before DT
Delta Power (μV²)
2000
1000
0
EMG (a.u.)
1.2
0.0
REM
SWS
Wake
After DT
7 pm
7 am
Clock Time
Delta
6 pm

Figure 21. Ablation of AAN disrupts natural sleep.
(A) Left, viral-genetic strategy for specifically expressing diphtheria toxin receptor (DTR) in AAN and the layout of EEG and EMG electrodes.
(B) Left, experimental setup of EEG/EMG recording across day and night. Right, top, experimental design and the timing of DT injection. Right, bottom, representative image of AAN ablation after DT injection. DT, diphtheria toxin; 1W, 1-week after DT; 2W, 2-week after DT.
(C) Representative polysomnographic recording before (top) and after (bottom) DT treatment in AAN-DTR mice.

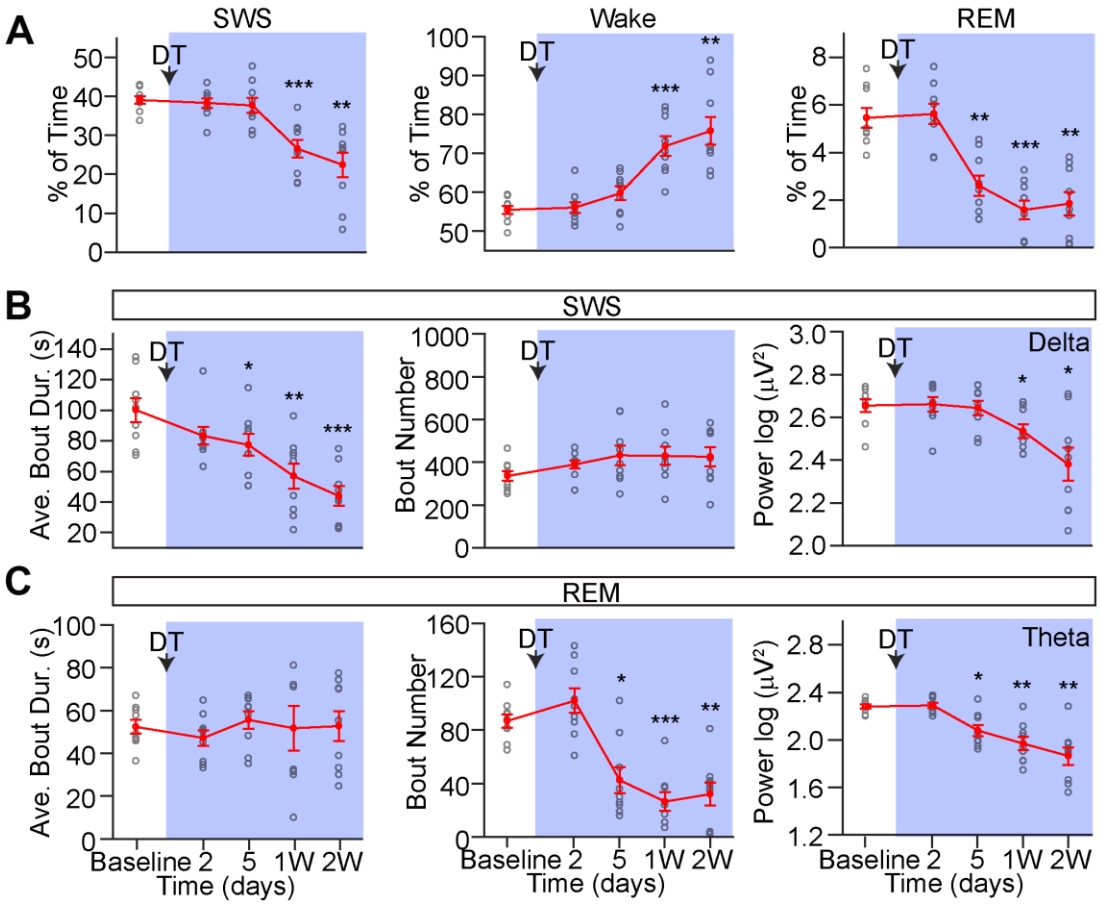
A
SWS
Wake
REM
% of Time
DT
B
SWS
Ave. Bout Dur. (s)
Bout Number
Power log (μV²)
Delta
C
REM
Theta
Baseline 2 5 1W 2W
Time (days)

Figure 22. Ablation of AAN disrupts natural sleep (Quantification).
(A) Total percentage of time spent in SWS (left), Wake (middle), and REM (right) across 23 hours recording. One-way repeated measures ANOVA followed by Sidak's post hoc test. n = 9 mice.
(B) Average bout duration, bout number and delta power of SWS. One-way repeated measures ANOVA followed by Sidak's post hoc test. n = 9 mice.
(C) Average bout duration, bout number and theta power of REM sleep. One-way repeated measures ANOVA followed by Sidak's post hoc test. n = 9 mice.
Data are presented as mean ± s.e.m. *P < 0.05, **P < 0.01, ***P < 0.001

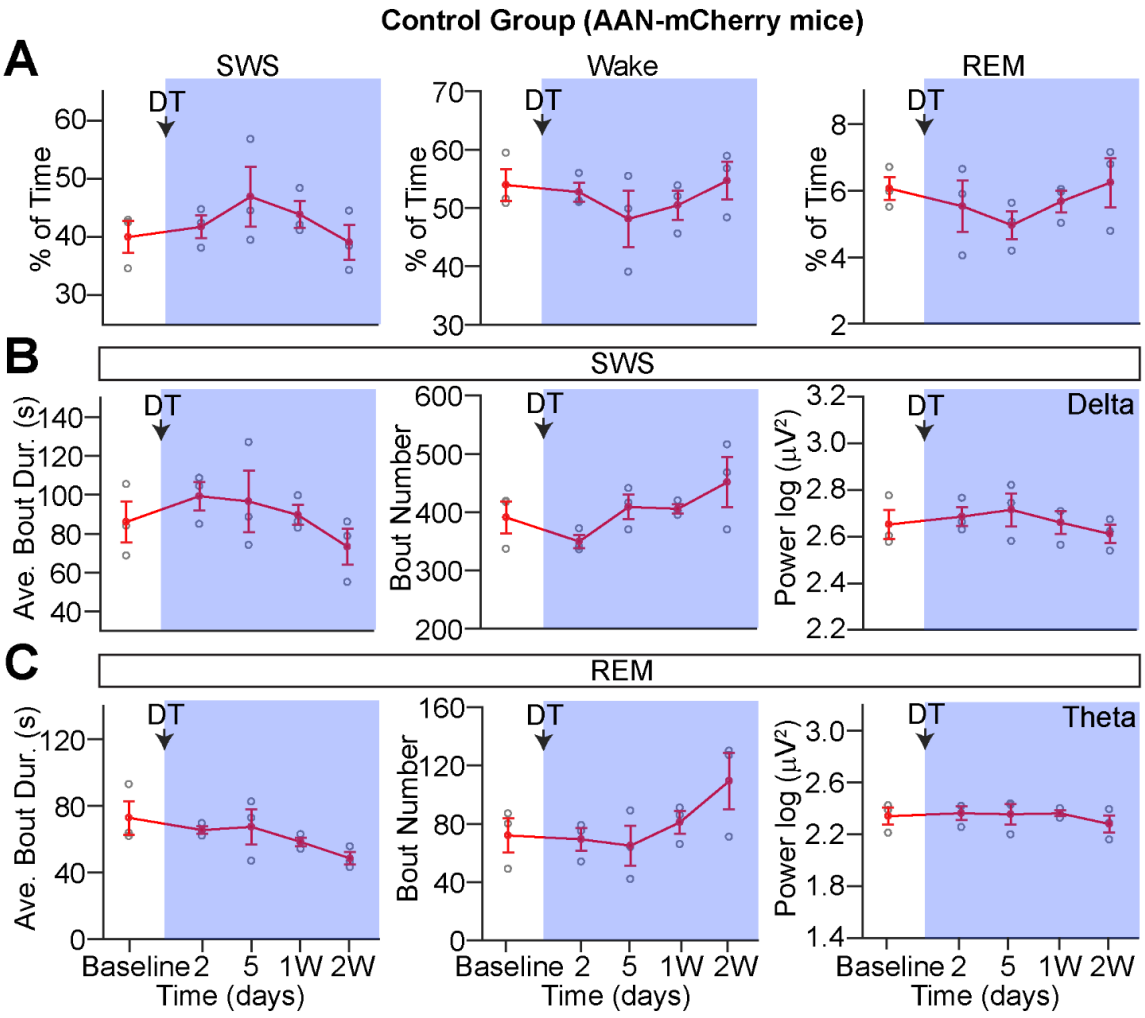

Figure 23. Diphtheria toxin (DT) in control AAN-mCherry mice.
(A) Total percentage of time in SWS (left), Wake (middle), and REM sleep (right).
(B) Average bout duration, bout numbers, and delta power of SWS.
(C) Average bout duration, bout number, and theta power of REM. One-way repeated measures ANOVA followed by Sidak's post hoc test. n = 3 mice.
Data are presented as mean ± s.e.m.

5.2 Optogenetic inhibition of AAN shortens the duration of GA

In the following, we had wanted to determine whether ablation of AAN could affect induction and duration of GA. However, DTR-mediated killing of AAN led to either mortality or chronic sleep loss, which are known to severely confound GA sensitivity (Tung et al., 2002). We therefore decided to perform acute silencing of AAN with chemogenetics or optogenetics. At the beginning, we tried to express inhibitory G-protein-coupled receptor hM4Di (Roth, 2016) in AAN with CANE technology. In ideal situations, this receptor would activate inwardly rectifying potassium (GIRK) channels thereby hyperpolarizing the membrane potential and attenuating neuronal activity. However, after introducing hM4Di into AAN, we performed ex vivo whole-cell patch-clamp electrophysiology, we surprisingly discovered that its ligand CNO do not even induced hyperpolarization of AAN. As a result, we speculated that AAN might have a distinct Gi pathway.

We thus turned to optogenetic strategy. The light-activated cation channel (AAN-eArch) (Chow et al., 2010) or control GFP (AAN-GFP) was expressed in AAN using CANE technology. Furthermore, we implanted of fiber optics (200 um) bilaterally above the AAN, and simultaneously placed EEG and EMG electrodes in the same animal (Figure 24). First, we validated that yellow-light (561nm) indeed induced sustained hyperpolarization of AAN expressing proton pump eArch3.0 (Figure 24B). For in vivo experiments, isoflurane (1%) was co-administered with yellow light (5 min square

pulse), the brain states of animals were monitored by EEG/EMG. Interestingly, we discovered inhibition of AAN did not alter GA induction, but significantly shortened the duration of GA (Figure 24C-F). These results, again, further underscore the importance of the slow but long-lasting peptidergic (and hormonal) signaling in maintaining and stabilizing the GA state.

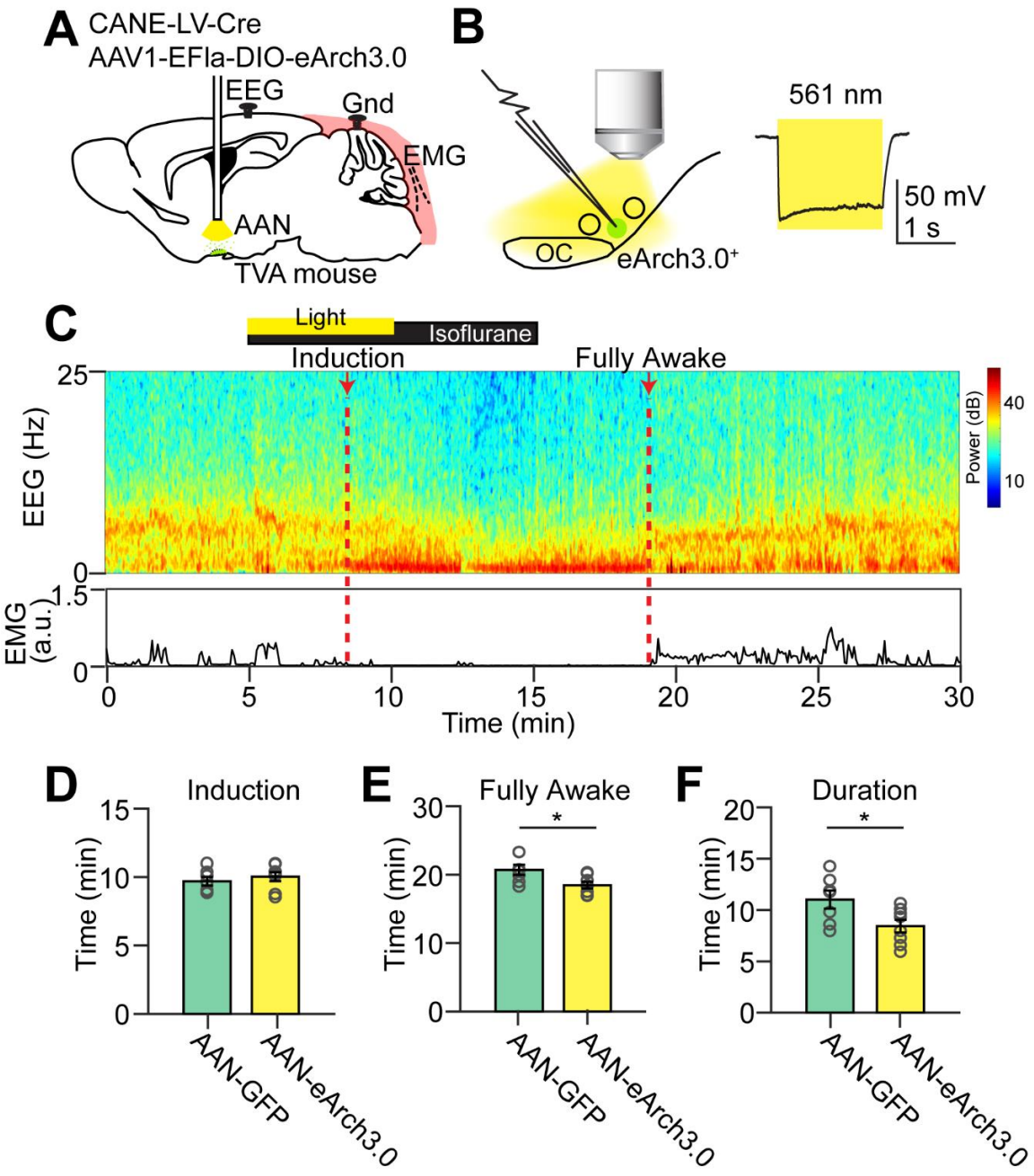
A
CANE-LV-Cre
AAV1-EFla-DIO-eArch3.0
EEG
Gnd
EMG
AAN
TVA mouse
B
561 nm
50 mV
1 s
OC
eArch3.0+
C
Light
Isoflurane
Induction
Fully Awake
EEG (Hz)
Power (dB)
EMG (a.u.)
Time (min)
D
Induction
E
Fully Awake
F
Duration
Time (min)
AAN-GFP
AAN-eArch3.0

Figure 24. Optogenetic inhibition of AAN shortens the duration of GA.
(A) Viral-genetic strategy for expressing eArch3.0 in AAN, the layout of optic fiber implantation, and EEG/EMG recording. Gnd, ground.
(B) Yellow light induces a sustained hyperpolarization in eArch3.0+ AAN. (C) Representative EEG/EMG recording across experimental session. Top, spectrogram of EEG; bottom, EMG. Isoflurane (1%) was infused for 10 min. Yellow laser stimulation (5 min square pulse, 5~7 mW measured at the fiber tips) was applied for the first 5 min of Isoflurane infusion. Induction time is identified by occurrence of slow oscillation and reduction of movement. Fully awake time is determined by reduction in slow wave power and raised muscle activity continuously for more than 1 min.
(D-F) Statistical analysis of Induction time (D), fully awake time (E), and anesthesia duration (F). n = 7 for AAN-GFP mice, n = 8 for AAN-eArch3.0 mice. Two-sample t-test. Data are presented as mean ± s.e.m., *P < 0.05.

5.3 Downstream targets of AAN

Finally, we reasoned that a complete map of the downstream targets of AAN would provide important clues for its biological function. We asked in addition to the posterior pituitary gland, a well-known axonal target of peptidergic SON neurons, whether AAN (both SON and paraSON) have any other downstream structure inside the brain. Here, GFP was expressed in AAN with the help of CANE technology. After the GFP was fully expressed, the brains of animals (n = 5) were collected, sectioned, and the axonal projections of AAN were visualized with confocal microscope throughout the entire mouse brain (Figure 25).

We found that AAN project to numerous brain regions that are involved in the generation of brain oscillations and regulation of sleep-wake behavior. For example, AAN innervated the septum, a structure known to pace the theta wave (6-10 Hz) of the hippocampus (Buzsaki, 2002), and the anterior thalamus, a brain region critical for modulating slow-wave activity in EEG (David et al., 2013). We also observed AAN axons in several brain areas engaged in arousal control, including posterior lateral hypothalamus (PLH) (Yamashita and Yamanaka, 2017), tuberomammillary nucleus (TMN) (Yu et al., 2015), supramammillary nucleus (MM) (Pedersen et al., 2017), lateral habenula (LHb) (Gelegen et al., 2018), periaqueductal gray (PAG) (Weber et al., 2018), ventral tegmental area (VTA) (Eban-Rothschild et al., 2016; Taylor et al., 2016), median raphe nucleus (MnR), pedunculopontine nucleus (PPTg), as well as laterodorsal

tegmental nucleus (LDTg) (Van Dort et al., 2015). It is interesting to note that lateral habenula (LHb) is one of AAN targets. A recent study discovered that activities of LHb excitatory neurons are required for natural sleep as well as for propofol-induced sedation (Gelegen et al., 2018). Finally, as expected, a large axon bundle was observed that travels towards the arcuate nucleus and median eminence (ARC-ME), which is the known axon pathway for SON axons en route to the posterior pituitary, where hormones are released to the general circulation.

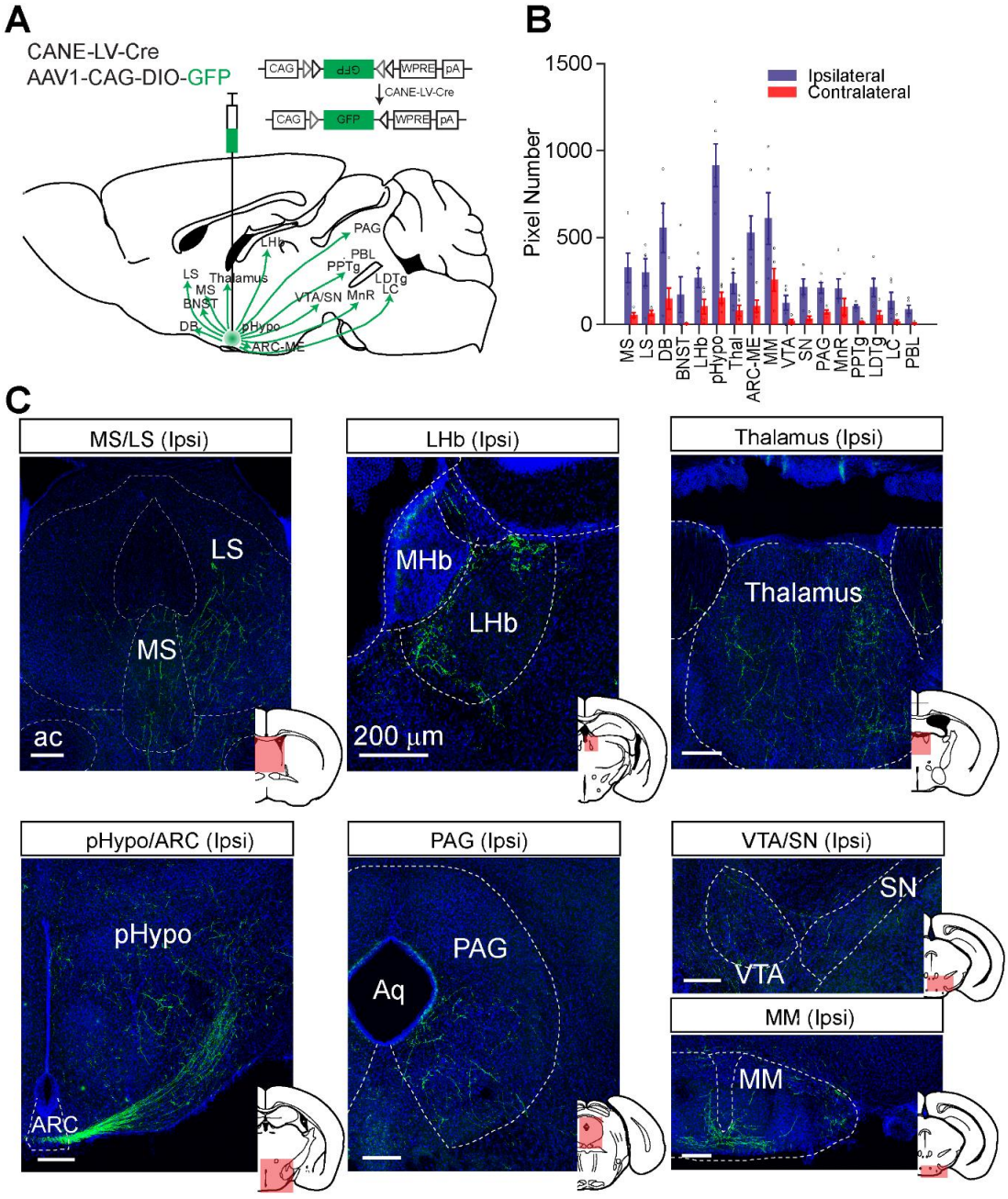
A
CANE-LV-Cre
AAV1-CAG-DIO-GFP
CAG
GFP
WPRE
pA
CANE-LV-Cre
CAG
GFP
WPRE
pA
PAG
LHb
PBL
PPTg
LDTg
LC
LS
Thalamus
MS
BNST
VTA/SN
MnR
DB
pHypo
ARC-ME
B
1500
1000
500
0
Pixel Number
Ipsilateral
Contralateral
MS
LS
DB
BNST
LHb
pHypo
Thal
ARC-ME
MM
VTA
SN
PAG
MnR
PPTg
LDTg
LC
PBL
C
MS/LS (Ipsi)
LS
MS
ac
LHb (Ipsi)
MHb
LHb
200 μm
Thalamus (Ipsi)
Thalamus
pHypo/ARC (Ipsi)
pHypo
ARC
PAG (Ipsi)
PAG
Aq
VTA/SN (Ipsi)
SN
VTA
MM (Ipsi)
MM

Figure 25. Projection targets of AAN

(A-B) Schematic summary of projection targets and quantification of projection densities of AAN. MS, medial septum; LS, lateral septum; DB, diagonal band of Broca; BNST, bed nucleus of the stria terminalis; LHb, lateral habenula; pHypo, posterior hypothalamus; Thal, thalamus; ARC-ME, arcuate nucleus-median eminence; MM, mammillary nucleus; VTA, ventral tegmental area; SN, substantia nigra; PAG, periaqueductal gray; MnR, median raphe nucleus; PPTg, pedunculopontine nucleus; LDTg, laterodorsal tegmental nucleus; LC, locus coeruleus; PBL, lateral parabrachial nucleus. n = 5 mice. Data are presented as mean ± s.e.m. (C) Representative images of projection targets. The shaded areas in the atlas indicate brain regions of interest. Green, AAN axon; Blue, DAPI.

6. Conclusions and future directions

Ever since the discovery of GA 170 years ago, the conventional view on GA drugs' mode of action is that they generally inhibit neuronal activities through targeting $GABA_A$ receptor or by weakening excitatory receptors (Rudolph and Antkowiak, 2004). Here, for the first time in literature, we demonstrate that chemically distinct GA drugs, from isoflurane, propofol, ketamine, to dexmedetomidine, all activate a common hypothalamic neural ensemble (AAN) composed mainly of peptidergic (AVP / Pdyn / Galanin) neuroendocrine cells in SON (Figure 6), as evidenced both in vitro in brain slice electrophysiology and in vivo multi-channel extracellular recording (Figures 1-4 and 11). Furthermore, optogenetic and chemogenetic activation of these AAN was sufficient to promote SWS by extending its duration and potentiate GA (Figures 12-15, 18-19), whereas ablating these AAN through selectively expressing DTR coupled with DT treatment, led to reduced slow-wave power, sleep fragmentation (reduced SWS bout duration), and loss of total sleep (both SWS and REM) (Figure 21-23). Furthermore, acute silencing of AAN with optogenetics shortened the duration of GA (Figure 24). Together, these results identify a previously unknown, yet common neural substrate at the intersection of sleep and GA. We believe these results would open a new avenue for future GA and sleep research.

6.1 The cellular mechanisms of activation of AAN by GA drugs

Although a couple of studies have claim to identify anesthesia-activated cells in several brain regions in recent years, all of them relied on indirect or in vitro methodologies, such as Fos labeling or brain slice recording (Gelegen et al., 2018; Lu et al., 2008; Moore et al., 2012; Zhang et al., 2015b). Here we were able to unequivocally demonstrate the presence of AAN in vivo through multi-channel extracellular recordings and simultaneous brain state monitoring through LFP and EMG (Figure 2-4). Most importantly, leveraging the fine temporal resolution afforded by electrophysiology, we were able to find that theses AAN could fire robustly and persistently during GA, and even fire ahead of the time when animals lose consciousness, while decrease their activity largely before the emergence from GA (Figure 3-4).

Furthermore, somewhat surprisingly, the AAN we discovered in this research can also be depolarized (activated) by multiple distinct classes of general anesthetics (Figure 9), although the underlying mechanisms were currently unknown. Interestingly, a recent study showed that GABA is actually excitatory even in adult SON AVP^+ cells due to intracellular Cl^- accumulation (Haam et al., 2012). Since a large number of general anesthetics were known to target $GABA_A$ receptors, we hypothesized that SON AAN (~85% of them are AVP^+ cells) could also be depolarized by other anesthetics as well. Intriguingly, during our exploration of optogenetic tools in this study, we also very

surprisingly observed that GtACR, light-gated chloride-conducting channelrhodopsin, could paradoxically drive excitation if we express it in AAN through CANE technology. These results collectively suggested that abnormal chloride concentration within AANs may be one potential mechanism for their persistent activation under GA.

Another very promising candidate is G protein-coupled receptors (GPCRs). GPCRs is extremely versatile in detecting various forms of chemicals, such as odors and tastes (Buck and Axel, 1991). Take my personal experience as an example, I realized my nose can assign distint odors to several volatile anesthetics which indicated the GPCRs on my olfactory sensory neurons could detect the GA drugs. Indeed, several studies in recent years discovered that a wide variety of general anesthetics (including halothane, isoflurane, sevoflurane, propofol, ketamine, and dexmedetomidine) could directly interact with GPCRs (Ho et al., 2015; Minami and Uezono, 2013). Interestingly, the downstream signaling pathway of excitatory GPCRs can increase intracellular calcium release from internal stores, and this calcium influx could further trigger neuropeptides and hormones release (Rosenbaum et al., 2009), we thus speculate that GA drugs may activate some GPCRs in AAN to produce depolarization. It will be an important future direction to identify the unknown GPCRs in these processes.

6.2 Neuroendocrine cells

During my doctoral studies, perhaps one of the most surprising findings is that the majority of AAN are actually peptidergic neuroendocrine cells located in SON (vasopressin$^+$ / dynorphin$^+$ / galanin$^+$ neurons). Previous research has indicated some GA drugs would induced Fos expression in the neurons located at preoptic area instead (Lu et al., 2008; Moore et al., 2012). Intriguingly, magnocellular SON neurons combine the properties of classical neurons and canonical endocrine cells (Leng, 2018) (Figure 16). Their axons travel all the way to the pituitary gland, while their dendrites cover major areas of the posterior hypothalamus. They have two modes of action. First, as neurons, they could generate action potentials to trigger hormone release from the pituitary gland into general circulation; second, as endocrine cells, they directly release neuropeptides from their dendrites and somas in large amount. Amazingly, within the cerebrospinal fluid, the concentration of peptides detected is high enough to activate targeted receptors in very distant brain regions (Ludwig and Leng, 2006). Thus, we reasoned neuroendocrine cells are ideally positioned to jointly regulate both brain and body state. Several recent studies also highlight the importance of neuroendocrine system in regulation of sleep with other model organisms, such as Caenorhabditis elegans (Anafi et al., 2019; Davis and Raizen, 2017) and Drosophila melanogaster (Davis and Raizen, 2017; Toda et al., 2019).

6.3 Neuropeptides

Although previous research largely focuses on fast inhibitory neurotransmitter GABA, our study, for the first time, highlights the importance of slow, global, and long-lasting peptidergic signaling in the regulation of GA. Very intriguingly, our results reveal there are at least two separable mechanisms of GA since chemogenetic and optogenetic manipulation of AAN only change the duration rather than the induction of GA. For the induction of GA, fast GABA signaling might be required to exert its effect; while for the maintenance of GA, systematic peptidergic signaling may play a much larger role. Interestingly, our manipulation of AAN only affect the duration instead of the frequency of SWS. We reasoned that the initiation and maintenance of sleep may also be regulated by distinct mechanisms.

Once we realized a large fraction of AAN is actually neuroendocrine cells, a crucial question following is to identify the neuropeptides expressed in these neurons. Our results indicate that AAN indeed express numerous peptides, mainly AVP, Pdyn, and galanin (Figure 6). Interestingly, these neuropeptides have been implicated in the sleep process and numerous physiological functions associated with sleep. For example, it has been shown that the secretion of vasopressin into general circulation from SON neurons typically increase during the hours of sleep both in human and rodents (Forsling, 1993; Trudel and Bourque, 2010), and enhanced AVP release was implicated in preventing dehydration (Trudel and Bourque, 2010) and lowering body temperature (Hicks et al.,

2014) during sleep. In addition, AVP also regulate the water channel aquaporin-4 in the central nervous system which is highly expressed in astrocytes and is a key component of the glymphatic system that has been implicated in driving metabolism clearance during natural sleep (Niermann et al., 2001; Xie et al., 2013). Furthermore, it has been shown that Dynorphin (encoded by Pdyn gene), when directly infused into anterior hypothalamus, has the potential to drastically increase the duration of SWS (Greco et al., 2008). Galanin and its homolog have been shown to promote sleep in several species, including fish, fly, and mice (Chen et al., 2017; Donlea et al., 2018; Kroeger et al., 2018). Thus, these peptides could potentially regulate multiple aspects of brain and body physiology required for promoting and sustaining sleep.

However, an important direction for future investigation is to directly measure the neuropeptides release in the brain during GA and natural sleep. Traditional approaches, such as microdialysis, might not be sensitive enough to detect trace amount of peptide release in the central nervous system. Recently, the development of several genetic-encoded-optical sensors for numerous neuromodulators (Feng et al., 2019; Jing et al., 2018; Patriarchi et al., 2018; Sun et al., 2018) provides a new hope for this line of investigation. Interestingly, a recent sequencing study has identified SON as one of the most genetically heterogenous tissues in the body (Mure et al., 2018), thus other as yet unidentified neuropeptides or neuromodulators might participate in promoting sleep. On the other hand, AAN also express vGlut2 (albeit at very low levels), and glutamate

released by these cells could potentially play a role in promoting sleep through activating downstream targets, a possibility awaiting future investigations.

6.4 Sleep pressure and homeostasis

Very surprisingly, we discovered that, in addition to activation by multiple distinct general anesthetics (Figure 9), AAN also respond strongly to sleep pressure (Figure 20). Although largely ignored, previous studies had demonstrated that endogenous somnogen prostaglandin D2 (PGD_2) and interleukin-6 could strongly activate SON neurons (Palin et al., 2009; Scammell et al., 1998). Proinflammatory cytokines, such as interleukin-1 beta (IL1 beta) and tumor necrosis factor alpha (TNF alpha), which are endogenously potent sleep-promoting molecules, also strongly induced Fos expression in SON neurons (Chang et al., 1993; Zielinski et al., 2013). In addition, utilizing amino-cupric-silver staining, a previous study also revealed that SON is the most affected region in prolonged sleep deprivation (Eiland et al., 2002). Thus, SON AAN might not be activated by sleep itself, but by the drive to sleep. Once been activated, AAN might release peptides or neuromodulators to stabilize subsequent sleep.

Furthermore, SON has been shown to highly express prostaglandin-H2 D-isomerase (PTGDS) (Mure et al., 2018), which convert prostaglandin H_2 to PGD_2, and secrete the precursor of adenosine, ATP (Brown et al., 2008). It is interesting to know the receptor for PGD_2 is directly located below the SON neurons in arachnoid trabecular cells of basal forebrain (Mizoguchi et al., 2001). Both PGD2 and adenosine are elevated

in sleep-deprived animals, and intracerebroventricular infusion of these molecules potentiates SWS but not REM sleep (Bjorness and Greene, 2009; Urade and Hayaishi, 2011). This is also consistent with our finding that a brief optogenetic stimulation of AAN is sufficient to strongly promote SWS in post-stimulation period (Figure 18).

More than a century ago, it was found that the cerebrospinal fluid of sleep deprived animals could promote sleep in other un-deprived animals (Kubota, 1989). It is conceivable that AAN could release peptides, neuromodulator, or other small molecules into cerebrospinal fluid through dendrites or somas in proportion to the sleep pressure. Since the receptors for these molecules may be widely expressed in the central nervous system, these neuropeptides can influence brain-wide neural activities and work on a longer time scale than classic neurotransmitters, which is required for globally coordinating the multiple brain regions to enter into the sleep as well as unconscious state induced by GA.

Although previous sleep research largely assumed that sleep-promoting neurons only activate during sleep, our study points to another possibility, sleep-promoting neurons may actually activate during prolong sleep deprivation, we name these neurons "sleep driver". In fact, activation of AAN by sleep drive instead of sleep per se would be in accordance with other innate homeostatic systems, such as feeding and drinking. During the past decade, it has been known neurons that promote feeding (Agrp+ cells in ARC) and drinking (Nos+ cells in the subfornical organ) are not activated by eating or

drinking itself, but by the desire to eat (hunger) or drink (thirst). Their activities actually reach maximal during prolong food or water deprived, and decreases almost immediately after a source of food or water appears (Betley et al., 2015; Zimmerman et al., 2017). We speculated that homeostatic regulation of sleep-wake behavior may thus follow the same logic. Future investigation is needed to carefully determine whether AAN play a critical role in homeostatic regulation of sleep and to determine which peptides or small molecules the AAN release into the brain (or body) once being activated by sleep pressure or general anesthetics.

6.5 Final conclusion

Taken together, our results reveal a common and previously unknown neuroendocrine substrate that is activated by multiple classes of anesthetic drugs, from Isoflurane, Propofol, Ketamine, to dexmedetomidine. Our data provide the first strong evidence that GA could work through activating instead of inhibiting neurons. We believe this biological insight would change the way we think of GA both in scientific and clinical settings. Furthermore, the CANE technology we utilized in this study would definitely inspire other scientists to identify, capture, and manipulate other anesthesia-activated neurons buried in several brain regions. These results also bring the previously known neuroendocrine system to the forefront of both clinical investigation and scientific research in GA as well as sleep medicine.

Appendix A: Experimental Methods

Animals

Adult male FosTVA knock-in mice (Sakurai et al., 2016) were used in this study (now available from JAX stock #027831). Adult AVP-IRES-Cre (JAX stock #023530) and C57BL/6 mice could be obtained from Jackson Laboratory. For chemogenetic activation of AVP neurons in SON, adult male heterozygous $AVP^{Cre/+}$ mice were used. For genetic labelling of anesthesia-activated neurons with CANE technology, adult Fos^{TVA} mice were single-house for 2~3 days to quench the background c-fos expression. Subjects were randomly assigned to experimental and control groups. Animals were housed in standard 12-h dark/12-h light cycle at common facility and all experimental procedures were approved by Duke Animal Care and Use Program.

Source of viral vectors

The CANE-LV-Cre was generated as previously described (Sakurai et al., 2016). Cre-inducible AAV vectors AAV8-hSyn-DIO-hM3D (Gq)-mCherry and AAV8-hSyn-DIO-mCherry, AAV1-EF1a-DIO-hChR2 (H134R)-EYFP were purchased from Addgene. AAV1-CAG-DIO-GFP and AAV1-EF1a-DIO-eArch3.0-EYFP were purchased from the University of North Carolina (UNC) Vector Core. AAV8-hSyn-DIO-DTR was produced by the viral vector core of the Boston Children's Hospital.

Immunofluorescence

After acutely anesthetized with isoflurane, mice were transcardially perfused with PBS (pH7.4), followed by ice-cold 4% paraformaldehyde (PFA) in PBS. The dissected brains were further post-fixed overnight in 4% PFA at 4 °C, and then transferred into 30% sucrose PBS buffer for 48 hours. Later, the brains were frozen in Tissue-Tek O.C.T. Compound (Sakura) and sliced at 60 um with cryostat (Leica Biosystems). The sections were washed with PBS, incubated with 1% Triton in PBS at room temperature for 1 hour, and applied with blocking solution (10% Blocking One in PBS with 0.3% Triton X-100) at room temperature for 1 h. Then, the sections were treated with appropriate primary antibodies with desired concentration in blocking solution at 4 °C for overnight. After washed by PBS three times, the sections were incubated with secondary antibody at 4 °C for another night. The sections were further washed, mounted and cover-slipped. The primary antibodies used in this study are: goat anti-Fos (Santa Cruz Biotechnology, sc52-g, 1:300). The secondary antibodies are: Alexa Fluor 488 donkey anti-goat (Jackson immunoresearch, 705-545-147 1:400).

Two-color in situ hybridization

The cDNA fragments of mouse c-fos, vGlut2, vGat, prodynorphin, and oxytocin, vasopressin, and galanin were amplified by PCR with the antisense primer incorporating the T7 promoter sequence. In vitro transcription was then performed

based on the PCR-amplified template using T7 RNA polymerase with DIG-UTP (Roche) or fluorescein-UTP (Roche) for the synthesis of the antisense probes. After hybridization and washing as the protocols we previously described (Bellavance et al., 2017; Zhang et al., 2015a), sections were first incubated with alkaline phosphatase–conjugated anti-DIG (1:3500, Roche) and developed with Fast Red substrate (Sigma). Subsequently, the sections were further incubated with POD anti-FITC (1:500, Roche), and developed with FITC-TSA (PerkinElmer).

Capturing anesthesia-activated neurons using CANE

Adult Fos^{TVA} (more than 8-week old) mice were single-house for two days to quench the background c-fos expression. On the third day, mice were first put under sustained GA (1~1.2% isoflurane) for 1.5 hours, then a stereotaxic surgery was performed, CANE-LV-Cre (500-750 nl) mixed with desired virus (see below) were co-injected into unilateral or bilateral AAN target area (AP 0.0, ML ±1, DV -5.30~5.40 from the Bregma). For axon-tracing experiment, AAV1-CAG-DIO-GFP (300-500 nl) was co-injected; for AAN labeling and recording, either AAV8-hSyn-DIO-mCherry (500 nl) or AAV1-CAG-DIO-GFP (500 nl) was co-injected; for chemogenetic activation or control experiments, AAV8-hSyn-DIO-hM3D (Gq)-mCherry (500 nl) or AAV8-hSyn-DIO-mCherry (500 nl) was co-injected; for optogenetic activation and inhibition, AAV1-EF1a-DIO-hChR2 (H134R)-EYFP and AAV1-EF1a-DIO-eArch3.0-EYFP were co-injected; for AAN ablation, AAV8-

hSyn-DIO-DTR (500 nl) was co-injected. ParaSON is defined as a brain region located within 500 um radius circle with the up-corner of the optic chiasm/tract as the center, extending from anterior to posterior hypothalamus.

Labelling of neuroendocrine cells with fluorogold injection

To identify neuroendocrine cells, we adapt the protocol as previous described (Kriegsfeld et al., 2003; Oyola et al., 2017). Briefly, mice were injected subcutaneously with 50 ul of 5% Fluorogold (Fluorochrome, Denver, Colorado) in saline. Five to six days later, animals were transcardially perfused with PBS, followed by 4% PFA. The brains were further removed, postfixed overnight, sectioned at 60 um with cryostat, and the images were taken with Zeiss 700 laser scanning confocal microscopy.

Axon-tracing and quantification

CANE-LV-Cre (500 nl) and AAV1-CAG-DIO-GFP (300-500 nl) were co-injected into AAN region of adult Fos^{TVA} mice. After the viral constructs fully expressed, mice were then sacrificed, the brain were cut into serial 80 um sections with cryostat (Leica Biosystems). The images were taken with Zeiss 700 laser scanning confocal microscopy. We adopted a similar strategy used by Allen Brain Institute to quantify AAN projection (Oh et al., 2014). In brief, GFP intensity were first normalized and binarized with a custom-written MATLAB code. Region of interests (ROI) were manually defined with

respect to standard atlas. GFP positive pixels and total number of pixels in each ROI were quantified.

Multi-channel in vivo recording and data analysis

Custom-built microelectrode array with 3~4 electrode bundles (30 um diameter tungsten, California Fine Wire) and two EMG wires (Stablohm 650, California Fine Wire) were constructed as previously described. One wire bundle (with 9 wires) were placed into AAN region (AP: 0.0, ML: ±1.00, DV: -5.40~5.50) to record the single-unit activity. Another bundle (with 6 wires) were placed into frontal cortex (AP: 1.70, ML: ±0.30, DV: -2.00) to capture brain oscillations. EMG wires were inserted into neck muscles. Mice were allowed to recover at least ten days before experiments. For each experimental session, mice were placed in the recording chamber connected with standard Isoflurane vaporizer. After initial 5 min of baseline recording (continuously infused with oxygen), isoflurane (1~1.2%) was applied into the chamber for 10 min, then the mice were allowed to emerge from GA for another 20 min. Neuronal spikes, local field potential, and muscle activity were recorded with CerePlex Direct (BlackRock Microsystem). Brain states were determined by frontal cortex neural oscillations and EMG activity. Spike-sorting were manually done with Offline Sorter (Plexon) based on principal component analysis (PCA). Single-units were identified with distinct clusters (nicely separated from

other units and noise) in PCA space and shown clear refractory period in autocorrelation histograms.

Units were classified into three categories based on the responsive property toward isoflurane exposure. Since the mice typically lose consciousness around 400 sec (100 sec after 1~1.2% Isoflurane infusion) and wake up around 1000~1400 sec (100~500 sec after Isoflurane withdraw) with 10 min total duration of isoflurane exposure, we calculated average spike rate for each unit during 400~1200 sec and compared with baseline spike rate of wakefulness 0~400 sec. Units with mean spike rate increase more than double (> 2) were identified as isoflurane-activated cells, while units with mean spike rate decrease more than a half (< 1/2) were classified as isoflurane-suppressed cells. The rest were weak-modulated cells. For illustration purpose, the spike rate of each unit was smoothed with gaussian kernel and normalized with peak firing rate. To capture the neuronal dynamics across brain state transitions (LOC and Emergence), spike density function (SDF) for each neuron is built by convolving Gaussian kernels (1 s-length for main Figure 3, 0.3 s- and 3 s-length for Figure 4) with raw spike train.

Slice electrophysiology

Coronal slices of hypothalamus were prepared from the adult male AAN-mCherry mice. Animals were briefly anesthetized with 1.2% isoflurane and then killed by

decapitation, and brain tissues were immediately dissected out and immersed in ice-cold oxygenated (95% O2 and 5% CO2) slicing solution in which isotonic sucrose was used as a substitute for NaCl (2.5 KCl, 1.25 NaH2PO4, 25 NaHCO3, 7 MgCl2, 0.5 CaCl2, 7 dextrose, 210 sucrose, 3 sodium pyruvate, 1.3 ascorbic acid). Slices (250 μm in thickness) were cut with a Leica microtome (VT-1000s, Leica, Germany) and immediately transferred to an incubation beaker filled with aerated holding solution: 125 NaCl, 2.5 KCl, 1.25 NaH2PO4, 25 NaHCO3, 2 MgCl2, 2 CaCl2, 12.5 dextrose, 3 sodium pyruvate, 1.3 ascorbic acid. After about 60-min incubation, we transferred slices to a submerged chamber perfused with aerated normal ACSF containing (in mM): 124 NaCl, 2.5 KCl, 1.25 NaH2PO4, 26 NaHCO3, 2 MgSO4, 2.5 CaCl2, 10 dextrose (315 mOsm, pH 7.4) and visualized by infrared differential interference contrast and fluorescence video microscopy (Examiner.D1, Zeiss). The patch-clamp electrode (4–6 MΩ) was filled with an intracellular solution containing 130 K-gluconate, 5 NaCl, 10 phosphocreatine disodium salt, 1 MgCl2, 10 HEPES, 0.02 EGTA, 0.5 Na2GTP, 2 MgATP, and 0.1% biocytin (pH 7.3, 280-290 mOsm). We employed a MultiClamp 700B amplifier (Molecular Devices) for patch-clamp recording and Spike2 software (Cambridge Electronic Design) for data acquisition. Non-volatile drugs propofol (15 uM, D126608, sigma), Ketamine (100 uM, Henry Schein), dexmedetomidine hydrochloride (40 uM, SML0956, sigma) and CNO (10 uM, Sigma-Aldrich C0832) were diluted from stock in fresh oxygenated aCSF immediately prior to use. Volatile drugs, isoflurane (25 ul) was

sonicated into solution in preoxygenated aCSF (50 ml), then stored in a gas-tight syringe (New Era Pump Systems Inc.) to prevent evaporation.

Drug administration

For chemogenetic activation in freely behaving mice, Clozapine N-oxide (CNO, Sigma-Aldrich C0832) was dissolved in 0.2 ml vehicle solution (PBS with 0.3% DMSO) and administered intraperitoneally (3 mg per kg). Ketamine (100 mg per kg) with or without xylazine (10 mg per kg) were dissolved in PBS and injected intraperitoneally. Dexmedetomidine (Sigma-Aldrich, SML0956) was dissolved in PBS injected intraperitoneally (100 ug per kg). Propofol (Sigma-Aldrich, D126608) was dissolved in intra-lipid solution (I141, sigma) injected intraperitoneally (180 mg per kg). Diphtheria toxin (DT, Sigma-Aldrich, D0564) was dissolved in PBS and intraperitoneally injected (50 ug per kg).

EEG/EMG recording and analysis

After the recovery from virus injection surgery (3-4 weeks), mice were further implanted with EEG and EMG. For chemogenetic activation experiment, three stainless steel screws were placed on the frontal, parietal, and cerebellar cortex as EEG electrodes and two thin microwires (Stablohm 650, California Fine Wire) were inserted into bilateral neck muscles as EMG electrodes. For optogenetic activation, two optic fibers (200 um, NA,

0.39, Thorlab) were inserted on top of AAN (AP 0.0 ~ -0.3, ML ±1, DV -5.00 ~ 5.20 from the Bregma) two stainless steel screws were placed on the parietal cortex and cerebellum, and EMG were inserted into neck muscles. Both EEG and EMG were connected into Omnetics connectors and recorded with CerePlex Direct (BlackRock Microsystem) at 2000 Hz. For chemogenetic activation experiments, after habituation to the recording chambers (Med Associates), experimental sessions typically began at 21:00 (dark phase) after either vehicle or CNO injections. For optogenetic experiment, after habituation to the recording chamber, experiments were performed from 20:30 to 24:00. Two laser trains (10 Hz, 10 ms, 1s-ON and 1s-OFF, 3 min, 3~4 mW from the fiber tip, 473-nm Blue Laser, Cobolt, Sweden) were given per experimental trial with inter-trial interval of 1~1.5 hours. Each animal was tested for 2~3 experimental trials (4~6 pulse trains). Brain state was semi-automatically scored at 4-s epochs with custom-written Matlab code (MathWorks) by the researchers blinded to experimental treatments. Slow-wave sleep was defined as high delta (1-4 Hz) power in the EEG and low EMG activity; REM sleep was defined as high theta (6-10 Hz) power in the EEG with minimal EMG signals; wakefulness was identified as small amplitude and high frequency EEG with tonic EMG activity. Spectrograms were generated with multi-taper approach (Prerau et al., 2017). EEG power spectra were computed for consecutive 4-s windows within the frequency range of 0-50 Hz using the Fast Fourier Transform (FFT). The frequency

resolution was set at 0.25 Hz and the power of interested frequency was further divided by the total power.

For optogenetic activation experiments during general anesthesia, mice were first habituated to the recording chamber. Later, one train of laser pulse (10 Hz, 10 ms, 1s-ON and 1s-OFF, 3 min, 3~4 mW from the fiber tip) was given to the animals followed by 1% Isoflurane anesthesia for 12 min. For optogenetic inhibition experiments, yellow laser light (5-min square pulse, 5~7 mW measured at the fiber tip, 561-nm DPSS Laser, OptoEngine LLC, Utah) was delivered for the first 5 min of Isoflurane anesthesia (1% isoflurane for 10 min). The time of Induction was determined by the onset of strong slow-wave power in EEG and minimal muscle activity in EMG; the time point of Fully Awake was determined by diminished slow-wave power and re-appearance of movement continuously for at least 1 min; the total Duration of unconscious time was calculated by the time point of Fully Awake minus the time point of Induction.

For DT/DTR ablation experiment, commercially available EEG/EMG headmounts (Pinnacle Technology, #8201-SS) were used. The electrical signals were acquired at 1000 Hz with EEG/EMG system from Pinnacle Technology. After habituation to the recording chamber, experiments were typically begun at 19:00 and continued toward 18:00 on the next day (23 hours of continuous recordings). Brain states were scored at 10-s epochs by the researchers blinded to experimental treatments with software SIRENIA® SLEEP PRO (Pinnacle Technology). For EEG power bands analysis, the delta (1-4 Hz) power of

SWS and the theta (6-10 Hz) power of REM sleep are computed with FFT. For each mouse, the median values of power across all the corresponding windows are used for further statistical analysis.

Mild sleep deprivation and recovery

Mice were kept in their home cages with freely access to water and foods. Sleep deprivation typically began at the light phase from 9:00 to 14:00. Mice were kept awake by introducing novel objects, cage tapping and rotation every 30 min. Recovery sleep was allowed from 14:00 to 17:00. At the end of behavior sessions, Fos staining were performed as described above.

Quantification and statistical analysis

For paired observations in slice electrophysiology experiment, Wilcoxon signed-rank test was used to examine the difference between groups. For chemogenetic experiments, mice were randomly assigned to saline or CNO injection in counterbalance order, two-way repeated-measured ANOVA followed by Sidak's post hoc test (AAN-hM3Dq experiment) or paired t-test (AVP-hM3Dq) was used to assess the statistical difference. For optogenetic experiment, permutation tests (> 10000 iterations) were performed between AAN-ChR2 and AAN-GFP groups across SWS, Wake, REM. For general anesthesia induction experiment, two-sample t-test was used to compare AAN-GFP and

AAN-ChR2 groups, or to compare AAN-GFP and AAN-eArch3.0 groups. For DTR-ablation experiment, one-way repeated measures ANOVA followed by Sidak's post hoc test was used. Statistical analysis was conducted with Prism (GraphPad), SPSS (IBM) and Matlab (MathWorks). All data were presented as mean ± s.e.m. Error bars in figures also represent s.e.m. In addition, the power spectra of SWS and Wake were also plotted with 95% confidence interval in Figure S5. Indications of significance level are as follows: *$P < 0.05$; **$P < 0.01$, and ***$P < 0.001$.

References

Akeju, O., and Brown, E.N. (2017). Neural oscillations demonstrate that general anesthesia and sedative states are neurophysiologically distinct from sleep. Curr Opin Neurobiol *44*, 178-185.

Alkire, M.T., Hudetz, A.G., and Tononi, G. (2008). Consciousness and anesthesia. Science *322*, 876-880.

Anaclet, C., Lin, J.S., Vetrivelan, R., Krenzer, M., Vong, L., Fuller, P.M., and Lu, J. (2012). Identification and characterization of a sleep-active cell group in the rostral medullary brainstem. J Neurosci *32*, 17970-17976.

Anafi, R.C., Kayser, M.S., and Raizen, D.M. (2019). Exploring phylogeny to find the function of sleep. Nat Rev Neurosci *20*, 109-116.

Belelli, D., Lambert, J.J., Peters, J.A., Wafford, K., and Whiting, P.J. (1997). The interaction of the general anesthetic etomidate with the gamma-aminobutyric acid type A receptor is influenced by a single amino acid. Proc Natl Acad Sci U S A *94*, 11031-11036.

Bellavance, M.A., Takatoh, J., Lu, J., Demers, M., Kleinfeld, D., Wang, F., and Deschenes, M. (2017). Parallel Inhibitory and Excitatory Trigemino-Facial Feedback Circuitry for Reflexive Vibrissa Movement. Neuron *95*, 722-723.

Betley, J.N., Xu, S., Cao, Z.F.H., Gong, R., Magnus, C.J., Yu, Y., and Sternson, S.M. (2015). Neurons for hunger and thirst transmit a negative-valence teaching signal. Nature *521*, 180-185.

Bjorness, T.E., and Greene, R.W. (2009). Adenosine and sleep. Curr Neuropharmacol *7*, 238-245.

Boyden, E.S., Zhang, F., Bamberg, E., Nagel, G., and Deisseroth, K. (2005). Millisecond-timescale, genetically targeted optical control of neural activity. Nat Neurosci *8*, 1263-1268.

Brown, C.H., Ruan, M., Scott, V., Tobin, V.A., and Ludwig, M. (2008). Multi-factorial somato-dendritic regulation of phasic spike discharge in vasopressin neurons. Prog Brain Res *170*, 219-228.

Brown, E.N., Lydic, R., and Schiff, N.D. (2010). General anesthesia, sleep, and coma. N Engl J Med *363*, 2638-2650.

Buck, L., and Axel, R. (1991). A Novel Multigene Family May Encode Odorant Receptors - a Molecular-Basis for Odor Recognition. Cell *65*, 175-187.

Buzsaki, G. (2002). Theta oscillations in the hippocampus. Neuron *33*, 325-340.

Chang, S.L., Ren, T., and Zadina, J.E. (1993). Interleukin-1 activation of FOS proto-oncogene protein in the rat hypothalamus. Brain Res *617*, 123-130.

Chen, S., Reichert, S., Singh, C., Oikonomou, G., Rihel, J., and Prober, D.A. (2017). Light-Dependent Regulation of Sleep and Wake States by Prokineticin 2 in Zebrafish. Neuron *95*, 153-168 e156.

Chow, B.Y., Han, X., Dobry, A.S., Qian, X., Chuong, A.S., Li, M., Henninger, M.A., Belfort, G.M., Lin, Y., Monahan, P.E., *et al.* (2010). High-performance genetically targetable optical neural silencing by light-driven proton pumps. Nature *463*, 98-102.

Chung, S., Weber, F., Zhong, P., Tan, C.L., Nguyen, T.N., Beier, K.T., Hormann, N., Chang, W.C., Zhang, Z., Do, J.P., *et al.* (2017). Identification of preoptic sleep neurons using retrograde labelling and gene profiling. Nature *545*, 477-481.

Danskin, B., Denman, D., Valley, M., Ollerenshaw, D., Williams, D., Groblewski, P., Reid, C., Olsen, S., Blanche, T., and Waters, J. (2015). Optogenetics in Mice Performing a Visual Discrimination Task: Measurement and Suppression of Retinal Activation and the Resulting Behavioral Artifact. PLoS One *10*, e0144760.

David, F., Schmiedt, J.T., Taylor, H.L., Orban, G., Di Giovanni, G., Uebele, V.N., Renger, J.J., Lambert, R.C., Leresche, N., and Crunelli, V. (2013). Essential thalamic contribution to slow waves of natural sleep. J Neurosci *33*, 19599-19610.

Davis, K.C., and Raizen, D.M. (2017). A mechanism for sickness sleep: lessons from invertebrates. J Physiol *595*, 5415-5424.

Donlea, J.M., Pimentel, D., Talbot, C.B., Kempf, A., Omoto, J.J., Hartenstein, V., and Miesenbock, G. (2018). Recurrent Circuitry for Balancing Sleep Need and Sleep. Neuron *97*, 378-389 e374.

Dzirasa, K., Fuentes, R., Kumar, S., Potes, J.M., and Nicolelis, M.A. (2011). Chronic in vivo multi-circuit neurophysiological recordings in mice. J Neurosci Methods *195*, 36-46.

Eban-Rothschild, A., Rothschild, G., Giardino, W.J., Jones, J.R., and de Lecea, L. (2016). VTA dopaminergic neurons regulate ethologically relevant sleep-wake behaviors. Nat Neurosci *19*, 1356-1366.

Eiland, M.M., Ramanathan, L., Gulyani, S., Gilliland, M., Bergmann, B.M., Rechtschaffen, A., and Siegel, J.M. (2002). Increases in amino-cupric-silver staining of the supraoptic nucleus after sleep deprivation. Brain Res *945*, 1-8.

Everson, C.A., Bergmann, B.M., and Rechtschaffen, A. (1989). Sleep deprivation in the rat: III. Total sleep deprivation. Sleep *12*, 13-21.

Feng, J., Zhang, C., Lischinsky, J.E., Jing, M., Zhou, J., Wang, H., Zhang, Y., Dong, A., Wu, Z., Wu, H., *et al.* (2019). A Genetically Encoded Fluorescent Sensor for Rapid and Specific In Vivo Detection of Norepinephrine. Neuron *102*, 745-761 e748.

Forsling, M.L. (1993). Neurohypophysial hormones and circadian rhythm. Ann N Y Acad Sci *689*, 382-395.

Franks, N.P. (2008). General anaesthesia: from molecular targets to neuronal pathways of sleep and arousal. Nat Rev Neurosci *9*, 370-386.

Franks, N.P., and Lieb, W.R. (1988). Volatile general anaesthetics activate a novel neuronal K+ current. Nature *333*, 662-664.

Gelegen, C., Miracca, G., Ran, M.Z., Harding, E.C., Ye, Z., Yu, X., Tossell, K., Houston, C.M., Yustos, R., Hawkins, E.D., *et al.* (2018). Excitatory Pathways from the Lateral Habenula Enable Propofol-Induced Sedation. Curr Biol *28*, 580-587 e585.

Gomez, J.L., Bonaventura, J., Lesniak, W., Mathews, W.B., Sysa-Shah, P., Rodriguez, L.A., Ellis, R.J., Richie, C.T., Harvey, B.K., Dannals, R.F., *et al.* (2017). Chemogenetics revealed: DREADD occupancy and activation via converted clozapine. Science *357*, 503-507.

Greco, M.A., Fuller, P.M., Jhou, T.C., Martin-Schild, S., Zadina, J.E., Hu, Z., Shiromani, P., and Lu, J. (2008). Opioidergic projections to sleep-active neurons in the ventrolateral preoptic nucleus. Brain Res *1245*, 96-107.

Haam, J., Popescu, I.R., Morton, L.A., Halmos, K.C., Teruyama, R., Ueta, Y., and Tasker, J.G. (2012). GABA Is Excitatory in Adult Vasopressinergic Neuroendocrine Cells. Journal of Neuroscience *32*, 572-582.

Harris, J.A. (1998). Using c-fos as a neural marker of pain. Brain Res Bull *45*, 1-8.

Hicks, C., Ramos, L., Reekie, T., Misagh, G.H., Narlawar, R., Kassiou, M., and McGregor, I.S. (2014). Body temperature and cardiac changes induced by peripherally administered oxytocin, vasopressin and the non-peptide oxytocin receptor agonist WAY 267,464: a biotelemetry study in rats. Br J Pharmacol *171*, 2868-2887.

Ho, J., Perez-Aguilar, J.M., Gao, L., Saven, J.G., Matsunami, H., and Eckenhoff, R.G. (2015). Molecular recognition of ketamine by a subset of olfactory G protein-coupled receptors. Sci Signal *8*, ra33.

Jego, S., Glasgow, S.D., Herrera, C.G., Ekstrand, M., Reed, S.J., Boyce, R., Friedman, J., Burdakov, D., and Adamantidis, A.R. (2013). Optogenetic identification of a rapid eye movement sleep modulatory circuit in the hypothalamus. Nat Neurosci *16*, 1637-1643.

Jiang-Xie, L.F., Liao, H.M., Chen, C.H., Chen, Y.T., Ho, S.Y., Lu, D.H., Lee, L.J., Liou, H.H., Fu, W.M., and Gau, S.S. (2014). Autism-associated gene Dlgap2 mutant mice demonstrate exacerbated aggressive behaviors and orbitofrontal cortex deficits. Mol Autism *5*, 32.

Jiang-Xie, L.F., Yin, L., Zhao, S., Prevosto, V., Han, B.X., Dzirasa, K., and Wang, F. (2019). A Common Neuroendocrine Substrate for Diverse General Anesthetics and Sleep. Neuron *102*, 1053-1065 e1054.

Jing, M., Zhang, P., Wang, G., Feng, J., Mesik, L., Zeng, J., Jiang, H., Wang, S., Looby, J.C., Guagliardo, N.A., *et al.* (2018). A genetically encoded fluorescent acetylcholine indicator for in vitro and in vivo studies. Nat Biotechnol *36*, 726-737.

Kelz, M.B., Sun, Y., Chen, J., Cheng Meng, Q., Moore, J.T., Veasey, S.C., Dixon, S., Thornton, M., Funato, H., and Yanagisawa, M. (2008). An essential role for orexins in emergence from general anesthesia. Proc Natl Acad Sci U S A *105*, 1309-1314.

Kilduff, T.S., and Dan, Y. (2017). Editorial overview: Neurobiology of sleep 2017. Curr Opin Neurobiol *44*, A1-A3.

Koch, C., Massimini, M., Boly, M., and Tononi, G. (2016). Neural correlates of consciousness: progress and problems. Nat Rev Neurosci *17*, 307-321.

Kottler, B., Bao, H., Zalucki, O., Imlach, W., Troup, M., van Alphen, B., Paulk, A., Zhang, B., and van Swinderen, B. (2013). A sleep/wake circuit controls isoflurane sensitivity in Drosophila. Curr Biol *23*, 594-598.

Kriegsfeld, L.J., Korets, R., and Silver, R. (2003). Expression of the circadian clock gene Period 1 in neuroendocrine cells: an investigation using mice with a Per1::GFP transgene. Eur J Neurosci *17*, 212-220.

Kroeger, D., Absi, G., Gagliardi, C., Bandaru, S.S., Madara, J.C., Ferrari, L.L., Arrigoni, E., Munzberg, H., Scammell, T.E., Saper, C.B., *et al.* (2018). Galanin neurons in the ventrolateral preoptic area promote sleep and heat loss in mice. Nat Commun *9*, 4129.

Kubota, K. (1989). Kuniomi Ishimori and the first discovery of sleep-inducing substances in the brain. Neurosci Res *6*, 497-518.

Kung, J.C., Chen, T.C., Shyu, B.C., Hsiao, S., and Huang, A.C. (2010). Anxiety- and depressive-like responses and c-fos activity in preproenkephalin knockout mice: oversensitivity hypothesis of enkephalin deficit-induced posttraumatic stress disorder. J Biomed Sci *17*, 29.

Lee, D.A., Andreev, A., Truong, T.V., Chen, A., Hill, A.J., Oikonomou, G., Pham, U., Hong, Y.K., Tran, S., Glass, L., *et al.* (2017). Genetic and neuronal regulation of sleep by neuropeptide VF. Elife *6*.

Leng, G. (2018). The heart of the brain : the hypothalamus and its hormones (Cambridge, MA: The MIT Press).

Li, G., Warner, M., Lang, B.H., Huang, L., and Sun, L.S. (2009). Epidemiology of anesthesia-related mortality in the United States, 1999-2005. Anesthesiology *110*, 759-765.

Lin, Y., Bloodgood, B.L., Hauser, J.L., Lapan, A.D., Koon, A.C., Kim, T.K., Hu, L.S., Malik, A.N., and Greenberg, M.E. (2008). Activity-dependent regulation of inhibitory synapse development by Npas4. Nature *455*, 1198-1204.

Liu, X., Ramirez, S., Pang, P.T., Puryear, C.B., Govindarajan, A., Deisseroth, K., and Tonegawa, S. (2012). Optogenetic stimulation of a hippocampal engram activates fear memory recall. Nature *484*, 381-385.

Lu, J., Nelson, L.E., Franks, N., Maze, M., Chamberlin, N.L., and Saper, C.B. (2008). Role of endogenous sleep-wake and analgesic systems in anesthesia. J Comp Neurol *508*, 648-662.

Ludwig, M., and Leng, G. (2006). Dendritic peptide release and peptide-dependent behaviours. Nat Rev Neurosci *7*, 126-136.

Mihic, S.J., Ye, Q., Wick, M.J., Koltchine, V.V., Krasowski, M.D., Finn, S.E., Mascia, M.P., Valenzuela, C.F., Hanson, K.K., Greenblatt, E.P., *et al.* (1997). Sites of alcohol and volatile anaesthetic action on GABA(A) and glycine receptors. Nature *389*, 385-389.

Minami, K., and Uezono, Y. (2013). The recent progress in research on effects of anesthetics and analgesics on G protein-coupled receptors. J Anesth *27*, 284-292.

Mizoguchi, A., Eguchi, N., Kimura, K., Kiyohara, Y., Qu, W.M., Huang, Z.L., Mochizuki, T., Lazarus, M., Kobayashi, T., Kaneko, T., *et al.* (2001). Dominant localization of prostaglandin D receptors on arachnoid trabecular cells in mouse basal forebrain and their involvement in the regulation of non-rapid eye movement sleep. P Natl Acad Sci USA *98*, 11674-11679.

Moore, J.T., Chen, J., Han, B., Meng, Q.C., Veasey, S.C., Beck, S.G., and Kelz, M.B. (2012). Direct activation of sleep-promoting VLPO neurons by volatile anesthetics contributes to anesthetic hypnosis. Curr Biol *22*, 2008-2016.

Morgan, J.I., and Curran, T. (1989). Stimulus-transcription coupling in neurons: role of cellular immediate-early genes. Trends Neurosci *12*, 459-462.

Mure, L.S., Le, H.D., Benegiamo, G., Chang, M.W., Rios, L., Jillani, N., Ngotho, M., Kariuki, T., Dkhissi-Benyahya, O., Cooper, H.M., *et al.* (2018). Diurnal transcriptome atlas of a primate across major neural and peripheral tissues. Science.

Mutsuga, N., Shahar, T., Verbalis, J.G., Brownstein, M.J., Xiang, C.C., Bonner, R.F., and Gainer, H. (2004). Selective gene expression in magnocellular neurons in rat supraoptic nucleus. J Neurosci *24*, 7174-7185.

Niermann, H., Amiry-Moghaddam, M., Holthoff, K., Witte, O.W., and Ottersen, O.P. (2001). A novel role of vasopressin in the brain: modulation of activity-dependent water flux in the neocortex. J Neurosci *21*, 3045-3051.

Oh, S.W., Harris, J.A., Ng, L., Winslow, B., Cain, N., Mihalas, S., Wang, Q., Lau, C., Kuan, L., Henry, A.M., *et al.* (2014). A mesoscale connectome of the mouse brain. Nature *508*, 207-214.

Oyola, M.G., Thompson, M.K., Handa, A.Z., and Handa, R.J. (2017). Distribution and chemical composition of estrogen receptor beta neurons in the paraventricular nucleus of the female and male mouse hypothalamus. J Comp Neurol *525*, 3666-3682.

Pal, D., Dean, J.G., Liu, T., Li, D., Watson, C.J., Hudetz, A.G., and Mashour, G.A. (2018). Differential Role of Prefrontal and Parietal Cortices in Controlling Level of Consciousness. Curr Biol *28*, 2145-2152 e2145.

Palin, K., Moreau, M.L., Sauvant, J., Orcel, H., Nadjar, A., Duvoid-Guillou, A., Dudit, J., Rabie, A., and Moos, F. (2009). Interleukin-6 activates arginine vasopressin neurons in the supraoptic nucleus during immune challenge in rats. Am J Physiol Endocrinol Metab *296*, E1289-1299.

Patriarchi, T., Cho, J.R., Merten, K., Howe, M.W., Marley, A., Xiong, W.H., Folk, R.W., Broussard, G.J., Liang, R., Jang, M.J., *et al.* (2018). Ultrafast neuronal imaging of dopamine dynamics with designed genetically encoded sensors. Science *360*.

Pedersen, N.P., Ferrari, L., Venner, A., Wang, J.L., Abbott, S.B.G., Vujovic, N., Arrigoni, E., Saper, C.B., and Fuller, P.M. (2017). Supramammillary glutamate neurons are a key node of the arousal system. Nat Commun *8*, 1405.

Ponzio, T.A., Ni, Y., Montana, V., Parpura, V., and Hatton, G.I. (2006). Vesicular glutamate transporter expression in supraoptic neurones suggests a glutamatergic phenotype. J Neuroendocrinol *18*, 253-265.

Prerau, M.J., Brown, R.E., Bianchi, M.T., Ellenbogen, J.M., and Purdon, P.L. (2017). Sleep Neurophysiological Dynamics Through the Lens of Multitaper Spectral Analysis. Physiology (Bethesda) *32*, 60-92.

Robinson, D.H., and Toledo, A.H. (2012). Historical development of modern anesthesia. J Invest Surg *25*, 141-149.

Rosenbaum, D.M., Rasmussen, S.G., and Kobilka, B.K. (2009). The structure and function of G-protein-coupled receptors. Nature *459*, 356-363.

Roth, B.L. (2016). DREADDs for Neuroscientists. Neuron *89*, 683-694.

Rudolph, U., and Antkowiak, B. (2004). Molecular and neuronal substrates for general anaesthetics. Nat Rev Neurosci *5*, 709-720.

Saito, M., Iwawaki, T., Taya, C., Yonekawa, H., Noda, M., Inui, Y., Mekada, E., Kimata, Y., Tsuru, A., and Kohno, K. (2001). Diphtheria toxin receptor-mediated conditional and targeted cell ablation in transgenic mice. Nat Biotechnol *19*, 746-750.

Sakurai, K., Zhao, S., Takatoh, J., Rodriguez, E., Lu, J., Leavitt, A.D., Fu, M., Han, B.X., and Wang, F. (2016). Capturing and Manipulating Activated Neuronal Ensembles with CANE Delineates a Hypothalamic Social-Fear Circuit. Neuron *92*, 739-753.

Scammell, T., Gerashchenko, D., Urade, Y., Onoe, H., Saper, C., and Hayaishi, O. (1998). Activation of ventrolateral preoptic neurons by the somnogen prostaglandin D2. Proc Natl Acad Sci U S A *95*, 7754-7759.

Scammell, T.E., Arrigoni, E., and Lipton, J.O. (2017). Neural Circuitry of Wakefulness and Sleep. Neuron *93*, 747-765.

Sherin, J.E., Elmquist, J.K., Torrealba, F., and Saper, C.B. (1998). Innervation of histaminergic tuberomammillary neurons by GABAergic and galaninergic neurons in the ventrolateral preoptic nucleus of the rat. J Neurosci *18*, 4705-4721.

Sun, F., Zeng, J., Jing, M., Zhou, J., Feng, J., Owen, S.F., Luo, Y., Li, F., Wang, H., Yamaguchi, T., *et al.* (2018). A Genetically Encoded Fluorescent Sensor Enables Rapid and Specific Detection of Dopamine in Flies, Fish, and Mice. Cell *174*, 481-496 e419.

Taylor, N.E., Van Dort, C.J., Kenny, J.D., Pei, J., Guidera, J.A., Vlasov, K.Y., Lee, J.T., Boyden, E.S., Brown, E.N., and Solt, K. (2016). Optogenetic activation of dopamine neurons in the ventral tegmental area induces reanimation from general anesthesia. Proc Natl Acad Sci U S A.

Toda, H., Williams, J.A., Gulledge, M., and Sehgal, A. (2019). A sleep-inducing gene, nemuri, links sleep and immune function in Drosophila. Science *363*, 509-515.

Trudel, E., and Bourque, C.W. (2010). Central clock excites vasopressin neurons by waking osmosensory afferents during late sleep. Nat Neurosci *13*, 467-474.

Tung, A., Bergmann, B.M., Herrera, S., Cao, D., and Mendelson, W.B. (2004). Recovery from sleep deprivation occurs during propofol anesthesia. Anesthesiology *100*, 1419-1426.

Tung, A., Szafran, M.J., Bluhm, B., and Mendelson, W.B. (2002). Sleep deprivation potentiates the onset and duration of loss of righting reflex induced by propofol and isoflurane. Anesthesiology *97*, 906-911.

Urade, Y., and Hayaishi, O. (2011). Prostaglandin D2 and sleep/wake regulation. Sleep Med Rev *15*, 411-418.

Van Dort, C.J., Zachs, D.P., Kenny, J.D., Zheng, S., Goldblum, R.R., Gelwan, N.A., Ramos, D.M., Nolan, M.A., Wang, K., Weng, F.J., *et al.* (2015). Optogenetic activation of cholinergic neurons in the PPT or LDT induces REM sleep. Proc Natl Acad Sci U S A *112*, 584-589.

Vazey, E.M., and Aston-Jones, G. (2014). Designer receptor manipulations reveal a role of the locus coeruleus noradrenergic system in isoflurane general anesthesia. Proc Natl Acad Sci U S A *111*, 3859-3864.

Watson, S.J., Akil, H., Fischli, W., Goldstein, A., Zimmerman, E., Nilaver, G., and van wimersma Griedanus, T.B. (1982). Dynorphin and vasopressin: common localization in magnocellular neurons. Science *216*, 85-87.

Weber, F., and Dan, Y. (2016). Circuit-based interrogation of sleep control. Nature *538*, 51-59.

Weber, F., Hoang Do, J.P., Chung, S., Beier, K.T., Bikov, M., Saffari Doost, M., and Dan, Y. (2018). Regulation of REM and Non-REM Sleep by Periaqueductal GABAergic Neurons. Nat Commun *9*, 354.

Weiss, M.L., and Cobbett, P. (1992). Intravenous injection of Evans Blue labels magnocellular neuroendocrine cells of the rat supraoptic nucleus in situ and after dissociation. Neuroscience *48*, 383-395.

Xie, L., Kang, H., Xu, Q., Chen, M.J., Liao, Y., Thiyagarajan, M., O'Donnell, J., Christensen, D.J., Nicholson, C., Iliff, J.J., *et al.* (2013). Sleep drives metabolite clearance from the adult brain. Science *342*, 373-377.

Yamashita, T., and Yamanaka, A. (2017). Lateral hypothalamic circuits for sleep-wake control. Curr Opin Neurobiol *44*, 94-100.

Yizhar, O., Fenno, L.E., Davidson, T.J., Mogri, M., and Deisseroth, K. (2011). Optogenetics in neural systems. Neuron *71*, 9-34.

Yu, X., Ye, Z.W., Houston, C.M., Zecharia, A.Y., Ma, Y., Zhang, Z., Uygun, D.S., Parker, S., Vyssotski, A.L., Yustos, R., *et al.* (2015). Wakefulness Is Governed by GABA and Histamine Cotransmission. Neuron *87*, 164-178.

Zhang, Y., Zhao, S., Rodriguez, E., Takatoh, J., Han, B.X., Zhou, X., and Wang, F. (2015a). Identifying local and descending inputs for primary sensory neurons. J Clin Invest *125*, 3782-3794.

Zhang, Z., Ferretti, V., Guntan, I., Moro, A., Steinberg, E.A., Ye, Z., Zecharia, A.Y., Yu, X., Vyssotski, A.L., Brickley, S.G., *et al.* (2015b). Neuronal ensembles sufficient for recovery sleep and the sedative actions of alpha2 adrenergic agonists. Nat Neurosci *18*, 553-561.

Zielinski, M.R., Dunbrasky, D.L., Taishi, P., Souza, G., and Krueger, J.M. (2013). Vagotomy attenuates brain cytokines and sleep induced by peripherally administered tumor necrosis factor-alpha and lipopolysaccharide in mice. Sleep *36*, 1227-1238, 1238A.

Zimmerman, C.A., Leib, D.E., and Knight, Z.A. (2017). Neural circuits underlying thirst and fluid homeostasis. Nat Rev Neurosci *18*, 459-469.

Biography

Li-Feng Jiang-Xie was born in Taoyuan city, Taiwan. He received his B.S in Psychology from National Taiwan University on January 2012, and M.S. in Brain and Cognitive Sciences from National Taiwan University on July 2013. He obtained his Doctor of Philosophy in Department of Neurobiology at Duke University (August 2014-September 2019). He has published the following first-author articles, "A Common Neuroendocrine Substrate for Diverse General Anesthetics and Sleep" (Jiang-Xie et al., 2019) in **Neuron**, "Autism-associated Gene Dlgap2 Mutant Mice Demonstrate Exacerbated Aggressive Behaviors and Orbitofrontal Cortex Deficits" (Jiang-Xie et al., 2014) in **Molecular Autism**. He has received Dean's Award, Learning Reward Scholarship twice, and Student Travel Award from National Taiwan University. He has been nominated for the Young Investigator Awards for Pediatric Neuroscience in Taiwan and HHMI International Student Predoctoral Fellowship by Duke University. He is also a member of Society of Neuroscience.